Chapter 3
Wave Propagation Along Spiny Dendrites

The majority of excitatory synapses that occur in the cerebral cortex are located on tiny specialized protoplasmic protuberances called dendritic *spines* [607]; see Fig. 3.1. They typically occupy 20–70 % of the total dendritic membrane. Since the input impedance of a spine head is typically large, a small excitatory synaptic current can produce a large local depolarization. Moreover, the thin stem neck connecting the spine to the main body of the dendrite provides an axial resistance that partially decouples the spine-head dynamics from the dendritic tree. Hence, it has long been theorized that the dendritic spine is a favorable site for the initiation of an action potential [427, 572] and is thus a possible substrate for local computations [571]. Modeling studies also suggest that if the heads of dendritic spines have excitable membrane properties, then the spread of current from one spine along the dendrites could bring adjacent spines to their thresholds for impulse generation. The result would be a sequence of spine-head action potentials, representing a saltatory propagating wave in the distal dendritic branches [19, 129]. Calcium-imaging experiments provide strong evidence that the spine heads are endowed with voltage-dependent Na^+ and Ca^{2+} channels that can indeed support an all-or-nothing response to an excitatory synaptic input [694].

Early theoretical studies of spines also considered their potential role in synaptic plasticity and Hebbian learning. This was motivated by the idea that small changes in spine morphology, such as changes in the width of the spine neck, could lead to large changes in the amplitude of response to excitatory synaptic inputs on to the spine. It is now known that spines are rich in actin filaments, which have the capacity to drive such changes in spine shape [413]. Moreover, there is increasing experimental evidence that the growth and removal of spines provides an important substrate for structural changes during brain development [410, 480, 693]. It is less clear whether changes in spine morphology play a significant role in adult plasticity. Nevertheless, the basic geometry of a spine does provide an isolated biochemical microenvironment for Ca^{2+} to accumulate, and Ca^{2+} is thought to be a major chemical signal for the induction of synaptic plasticity [343, 462]. The dynamics of calcium diffusion in dendritic spines has been explored in a number of computational models [202, 283].

P.C. Bressloff, *Waves in Neural Media: From Single Neurons to Neural Fields*,
Lecture Notes on Mathematical Modelling in the Life Sciences,
DOI 10.1007/978-1-4614-8866-8_3,

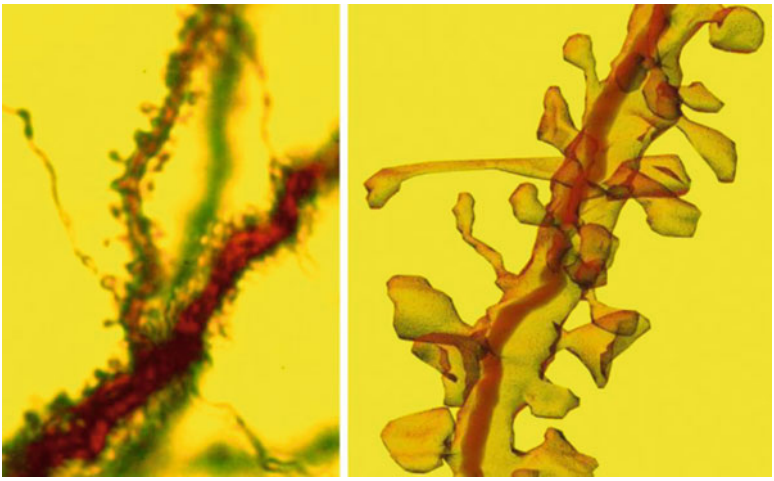

Fig. 3.1 An example of a piece of spine-studded dendritic tissue (from rat hippocampal region CA1 stratum radiatum). Magnified view on right-hand side shows a dendrite $\sim 5\,\mu$m in length. Taken with permission from SynapseWeb, Kristen M. Harris, PI, http://synapses.clm.utexas.edu/

Another important signaling molecule involved in the induction of synaptic plasticity is Ca^{2+}–calmodulin-dependent protein kinase II (CaMKII) [295, 386]. CaMKII is also found to be abundant within dendritic spines, where it can detect changes in the local levels of Ca^{2+} entering the synapse following plasticity-inducing stimuli, via binding of CaMKII to Ca^{2+}/CaM. Confinement of CaMKII within spines arises from the geometry of the spine and through interactions with protein receptors and cytoskeletal elements within the postsynaptic density (PSD), which is the protein-rich region at the tip of the spine head. Activated CaMKII phosphorylates substrates responsible for the expression of synaptic plasticity, namely, the number and the conductivity of synaptic AMPA receptors [151, 370]. Moreover, once activated, CaMKII can transition into a Ca^{2+}/CaM-independent, hyperactivated state via the autophosphorylation of neighboring enzymatic subunits and thus continue to phosphorylate its substrates even after the plasticity-inducing Ca^{2+} signal has ended [261, 427, 547, 689]. Experimentally, translocation of CaMKII into spines can be induced in a local region of dendrite by exposing it to a puff of glutamate, and this can initiate a wave of CaMKII translocation that spreads towards the distal end of the dendrite with an average speed of $\sim 1\,\mu$m/s [532]. It is found that the wave is preceded by a much faster Ca^{2+}-mediated spike that propagates along the dendrite (see above), which could provide a mechanism for priming CaMKII outside the stimulus region for diffusion-based activation. Moreover, the CaMKII translocation wave is associated with an increase in AMPA receptor numbers at both stimulated and nonstimulated synapses [532]. This suggests that it could provide a possible molecular substrate for heterosynaptic plasticity.

In this chapter we consider two mathematical models of wave propagation along spiny dendrites: (I) a spike–diffuse–spike model of spine-mediated spikes [129, 139] and (II) a reaction–diffusion model of CaMKII translocation waves [72, 161]. The former model introduces methods for analyzing solitary waves propagating in spiking networks; see also Sect. 5.4. The latter model turns out to be identical in form to the diffusive SI model introduced by Noble [464] to explain the spread of bubonic plague through Europe in the fourteenth century. This, in turn, is a generalization of the scalar Fisher–KPP equation [191, 345] which was originally introduced to model the invasion of a gene into a population. One characteristic feature of such equations is that they support traveling fronts propagating into an unstable steady state, in which the wave speed and longtime asymptotics are determined by the dynamics in the leading edge of the wave—so-called pulled fronts [544]. In particular, a sufficiently localized initial perturbation will asymptotically approach the traveling front solution that has the minimum possible wave speed. Hence, pulled fronts have very different properties from those found for the bistable equation in Sect. 2.2. Another important topic raised by these models is how to use homogenization methods to approximate the discrete distribution of spines by a smooth distribution.

3.1 Solitary Waves in a Spike–Diffuse–Spike Model of Active Spines

The first theoretical study of active wave propagation along a dendritic cable that is mediated by dendritic spines was carried out by Baer and Rinzel [19]. They considered a continuum model of a dendritic tree coupled to a distribution of excitable dendritic spines. The active spine-head dynamics is modeled with Hodgkin–Huxley kinetics, while the (distal) dendritic tissue is modeled with the cable equation. The spine head is coupled to the cable via a spine-stem resistance that delivers a current proportional to the number of spines at the contact point. There is no direct coupling between neighboring spines; voltage spread along the cable is the only way for spines to interact. Numerical studies of the Baer–Rinzel model [19] show both smooth and saltatory traveling wave solutions, the former arising in the case of uniform spine distributions and the latter when spines are clustered in groups. The saltatory nature of a propagating wave may be directly attributed to the fact that active spine clusters are physically separated. In this section we describe an alternative, analytically tractable treatment of saltatory waves based on the so-called spike–diffuse–spike (SDS) model of active dendritic spines [129, 138, 624, 625], which reduces the spine-head dynamics to an all-or-nothing action potential response.

In order to formulate the model, we first consider a continuum of spines with $\rho(x)$ representing the spine density per unit length along a uniform, passive dendritic cable. Denoting the voltage at position x on the cable at time t by $V = V(x,t)$, the associated cable equation is given by (see Sect. 1.4)

$$\frac{\partial V}{\partial t} = -\frac{V}{\tau_m} + D_m \frac{\partial^2 V}{\partial x^2} + \rho(x)\frac{a-V}{C_m r_s}, \tag{3.1}$$

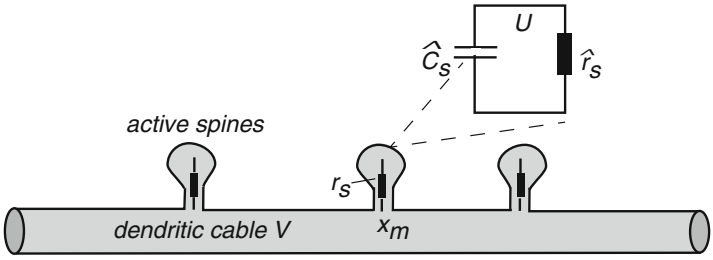

Fig. 3.2 Schematic diagram of a dendritic cable with active spines

where $D_m = \lambda_m^2/\tau_m$ with τ_m and λ_m the membrane time and space constants of the cable, C_m is the membrane capacitance per unit length, and r_s is the spine-stem resistance of an individual spine. In the SDS model, the function $a(x,t)$ represents the sequence of action potentials generated in the spine head at x whenever the associated subthreshold spine-head potential $U(x,t)$, driven by current from the shaft, crosses some threshold h. Given the high resistance of the spine stem, we neglect subthreshold currents into the cable. The voltage U evolves according to the integrate-and-fire (IF) equation (see Sect. 5.3)

$$\hat{C}_s \frac{\partial U}{\partial t} = -\frac{U}{\hat{r}_s} + \frac{V-U}{r_s}, \tag{3.2}$$

such that whenever U crosses the threshold h it is immediately reset to zero. Here $\hat{C}_s$ and $\hat{r}_s$ are the membrane capacitance and resistance of the spine head; see Fig. 3.2. Let $T^j(x)$ denote the jth firing time of the spine head at position x such that $U(x,T^j(x)) = h$. Then

$$a(x,t) = \sum_j \eta(t - T^j(x)), \tag{3.3}$$

with $\eta(t) = 0$ for all $t < 0$. The shape of the action potential is specified by the function $\eta(t)$, which can be fitted to the universal shape of an action potential.

3.1.1 Existence of a Solitary Wave for a Uniform Density

Let us begin by considering the simplest case of a uniform spine density $\rho(x) = \rho_0$ and a rectangular pulse shape of height η_0 and duration τ_d. We define a solitary wave as one that causes the spine head at x to reach threshold only once at the time $t = T(x) \equiv x/c$. We recognize c as the speed of the wave so that $a(x,t) = \eta(t - x/c)$, which suggests adopting a moving coordinate frame $\xi = ct - x$. Equation (3.1) becomes

$$D_m V_{\xi\xi}(\xi) - cV_\xi(\xi) - (\tau_m^{-1} + \beta)V(\xi) = -\beta a(\xi/c), \tag{3.4}$$

where $\beta = \rho_0/(C_m r_s)$, and

$$a(\xi) = \begin{cases} 0 & -\infty < \xi < 0 \\ \eta_0 & 0 < \xi < c\tau_d \\ 0 & \xi > c\tau_d. \end{cases} \tag{3.5}$$

If one is looking for traveling pulses which satisfy $\lim_{\xi\to\pm\infty} V(\xi) = 0$, then the solution to (3.4) takes the form

$$V(\xi) = \begin{cases} \alpha_1 \exp(m_+\xi), & -\infty < \xi < 0 \\ \alpha_2 \exp(m_+\xi) + \alpha_3 \exp(m_-\xi) + \frac{\beta\eta_0}{\tau_m^{-1}+\beta}, & 0 < \xi < c\tau_d \\ \alpha_4 \exp(m_-\xi), & \xi > c\tau_d \end{cases} \tag{3.6}$$

with

$$m_\pm = \frac{c \pm \sqrt{c^2 + 4D_m(\tau_m^{-1}+\beta)}}{2D_m}. \tag{3.7}$$

By ensuring the continuity of the solution and its first derivative at $\xi = 0$ and $\xi = c\tau_d$ one may solve for the unknowns $\alpha_1 \ldots \alpha_4$ as

$$\alpha_1 = \alpha_3 \frac{m_-}{m_+}[1 - \exp(-m_+ c\tau_d)], \tag{3.8}$$

$$\alpha_2 = -\alpha_3 \frac{m_-}{m_+} \exp(-m_+ c\tau_d), \tag{3.9}$$

$$\alpha_3 = \frac{\beta\eta_0}{\tau_m^{-1}+\beta} \frac{m_+}{(m_- - m_+)}, \tag{3.10}$$

$$\alpha_4 = \alpha_3[1 - \exp(-m_- c\tau_d)]. \tag{3.11}$$

As yet the speed of the pulse is undetermined. However, by demanding that the IF process in the spine head reaches threshold at $\xi = 0$ and that $\lim_{\xi\to\pm\infty} U(\xi) = 0$, one can determine a self-consistent value for the speed of the traveling wave along similar lines to the analysis of solitary waves in one-dimensional networks of IF neurons [62, 63, 167]; see Sect. 5.4. In the traveling coordinate frame, (3.2) becomes

$$c\hat{C}_s U_\xi = -g_s U + \frac{V}{r_s} \tag{3.12}$$

with $U(0) = h$ and $g_s = r_s^{-1} + \hat{r}_s^{-1}$. This first-order system may be solved as

$$U(\xi) = \exp(-\xi/[c\hat{\tau}]) \left[h - \frac{1}{c\hat{C}_s r_s} \int_\xi^0 V(\xi') \exp(\xi'/[c\hat{\tau}]) d\xi' \right], \tag{3.13}$$

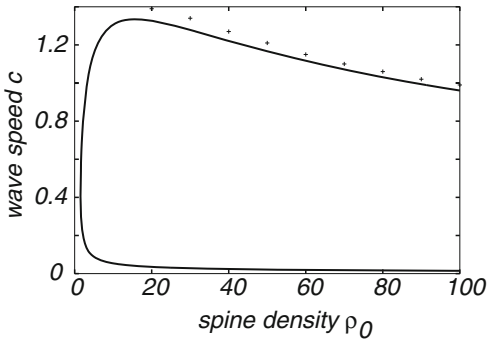

Fig. 3.3 Speed of a traveling pulse as a function of uniform spine density ρ_0 for $\tau_m = D_m = 1$, $h = 2.5$, $r_s = 2$, $\widehat{r_s} = 0.8$, $\hat{C}_s = 1$, $C_m = 1$, $\tau_d = 2$, $\eta_0 = 100$. The crosses show the results of a direct numerical simulation of the SDS model with $N = 200$ discrete spines uniformly distributed along a cable of length $L = 10$

where $\hat{\tau} = \hat{C}_s/g_s$. In order for this to be bounded as $\xi \to -\infty$, the term inside the large parentheses must vanish as $\xi \to -\infty$. This yields the dispersion relationship for the speed of the pulse as a function of system parameters:

$$h = \frac{1}{\hat{C}_s r_s} \frac{\alpha_1}{\hat{\tau}^{-1} + cm_+} \tag{3.14}$$

In Fig. 3.3 we plot dispersion curves for the speed c of a traveling pulse as a function of the spine density ρ_0, which are obtained by numerically solving (3.14). Note that there are two solution branches for a given density ρ_0. Direct simulations suggest that it is the upper (faster) branch that is stable, which can be confirmed analytically using linear stability analysis (see below). Figure 3.3 also shows that for a wide range of ρ_0 the speed of the stable wave is approximately λ_m/τ_m in physical units, in agreement with the original observations of Baer and Rinzel [19].

One useful feature of the SDS model is that it yields an exact expression for the speed of the wave that can easily be solved to obtain the dependence in terms of other system parameters such as the spine-stem resistance. Hence, one can find the minimum spine density capable of supporting a traveling pulse as well as extract information about how the speed decays as a function of spine density. In Fig. 3.4(a) we plot the speed of a traveling pulse as a function of the spine-stem resistance r_s. It is clear that for realistic choices of the biophysical parameters in the model, that propagation failure can occur for too large a choice of the spine-stem resistance. Moreover, for small r_s, the speed of a stable pulse is very sensitive to r_s, demonstrating that a modifiable value of the spine-stem resistance could have important ramifications for neural processing. Finally in Fig. 3.4(b) we show the dependence of the wave speed on the width, τ_d, of a rectangular pulse generated in the spine head. Interestingly, for a fixed pulse height, there is a minimum duration time below which propagation cannot occur. This highlights the fact that it is crucial to model the shape of an action potential in the reduced IF model with biologically realistic

choices for the amplitude and duration of the spine-head pulse. For large values of τ_d the speed of the wave approaches a constant value (i.e., the speed of the wave becomes insensitive to the precise choice of τ_d).

3.1.2 Linear Stability Analysis

For the purposes of linear stability analysis it is more convenient to work in terms of the original variables (x,t) rather than in the moving frame. Since the shape of the traveling pulse is fixed by the function $\eta(t)$, it is natural to consider local perturbations of the firing times given by $T(x) = x/c + \Delta(x)$. A similar approach is used to analyze the stability of traveling waves in IF networks with synaptic and passive dendritic interactions [62, 63]; see Sect. 5.4. The membrane potential $V(x,t)$ satisfying (3.1) with $a(t) = \eta(t - T(x))$ can be evaluated in terms of the Green's function G_0 for the infinite cable equation. That is, setting $C_m = 1$ and taking $\tau_m \gg \rho_0/r_s$,

$$V(x,t) = \frac{\rho_0}{r_s} \int_{-\infty}^{t} \left[\int_{-\infty}^{\infty} G_0(x-y, t-s)\eta(s - T(y))dy \right] ds \tag{3.15}$$

with G_0 given by (1.59). If we now demand that the IF process (3.2) driven by the potential $V(x,t)$ reaches threshold at time $T(x)$, then we obtain the following self-consistency condition for a traveling pulse (with $\hat{C}_s = 1$):

$$h = U(x, T(x)) = \frac{1}{r_s} \int_{-\infty}^{0} \mathrm{e}^{t/\hat{\tau}} V(x, t + T(x))dt. \tag{3.16}$$

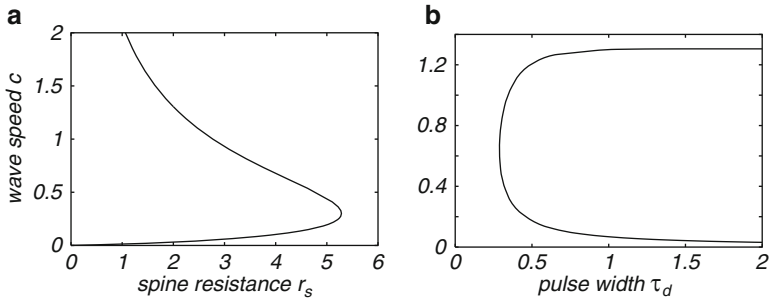

Fig. 3.4 (**a**) Speed of a traveling pulse as a function of spine-stem resistance r_s with $\rho_0 = 25$ and $\tau_d = 2$. (**b**) Speed of a traveling pulse as a function of pulse width τ_d with $\rho_0 = 25$ and $r_s = 2$. All other parameters are as Fig. 3.3. Note that for sufficiently large r_s or small τ_d solitary waves cannot propagate

We now expand (3.15) and (3.16) in powers of the perturbation $\Delta(x)$. The zeroth-order term generates the self-consistency condition for the speed c of the unperturbed traveling pulse:

$$h = \frac{1}{r_s}\int_{-\infty}^{0} e^{t/\hat{\tau}}\,\overline{V}(x,t+x/c)dt, \tag{3.17}$$

where

$$\overline{V}(x,t) = \frac{\rho_0}{r_s}\int_{-\infty}^{t}\left[\int_{-\infty}^{\infty} G_0(x-y,t-s)\eta(s-y/c)dy\right]ds. \tag{3.18}$$

We can evaluate (3.18) using Fourier transforms without needing to restrict η to be a rectangular pulse. That is, expand $\eta(s)$ as

$$\eta(t) = \int_{-\infty}^{\infty} e^{i\omega t}\tilde{\eta}(\omega)\frac{d\omega}{2\pi}, \tag{3.19}$$

and then perform the integrations over y and s with

$$\int_{-\infty}^{\infty} e^{-ikx}G_0(x,t)dx = e^{-\varepsilon(k)t}, \quad \varepsilon(k) = \tau_m^{-1} + D_m k^2, \tag{3.20}$$

to obtain

$$\overline{V}(x,t) = \frac{\rho_0}{r_s}\int_{-\infty}^{\infty} e^{i\omega(t-x/c)}\frac{\tilde{\eta}(\omega)}{\varepsilon(\omega/c)+i\omega}\frac{d\omega}{2\pi}. \tag{3.21}$$

Substitution of (3.21) into (3.17) finally gives

$$h = \frac{\rho_0}{r_s^2}\int_{-\infty}^{\infty}\frac{\tilde{\eta}(\omega)}{[\varepsilon(\omega/c)+i\omega][\hat{\tau}^{-1}+i\omega]}\frac{d\omega}{2\pi}. \tag{3.22}$$

When one considers a rectangular pulse shape for the action potential waveform of height η_0 and duration τ_d such that

$$\tilde{\eta}(\omega) = \eta_0\frac{1-e^{-i\omega\tau_d}}{i\omega}, \tag{3.23}$$

then it is a simple matter to check that the dispersion relationship (3.22) reduces to (3.14).

The first-order term in the expansion of (3.16) yields a linear equation for the perturbations $\Delta(x)$ from which the linear stability of the traveling pulse can be deduced. This linear equation takes the form

$$0 = \frac{1}{r_s}\int_{-\infty}^{0} e^{t/\hat{\tau}}\delta_\Delta V(x,t+x/c)dt, \tag{3.24}$$

where (after integration by parts)

$$\delta_\Delta V(x,t) = \frac{\rho_0}{r_s}\int_{-\infty}^{t}\left[\int_{-\infty}^{\infty} G_0(x-y,t-s)\eta'(s-y/c)[\Delta(x)-\Delta(y)]dy\right]ds. \tag{3.25}$$

Equations (3.24) and (3.25) have solutions of the form $\Delta(x) = e^{\lambda x}$ with λ satisfying the characteristic equation

$$I(\lambda) \equiv \int_{-\infty}^{\infty} \frac{ik\tilde{\eta}(\omega)}{[\varepsilon(\omega/c + i\lambda) + i\omega][\hat{\tau}^{-1} + i\omega]} \frac{d\omega}{2\pi} - I(0) = 0. \tag{3.26}$$

Asymptotic stability holds if all nonzero solutions of the characteristic equation have negative real part. (The existence of a solution $\lambda = 0$ reflects the translation invariance of the underlying system; see Sect. 2.4.) Equation (3.26) can be evaluated by closing the contour in the lower-half complex ω-plane. Since $\eta(s) = 0$ for $s < 0$ it follows that any poles of $\tilde{\eta}(\omega)$ lie in the upper-half complex plane so that we only have to consider poles arising from the zeros of the function $\varepsilon(\omega/c + i\lambda) + i\omega$. The latter are given explicitly by $\omega = i\omega_{\pm}(\lambda)$ where

$$\frac{\omega_{\pm}(\lambda)}{c} = -\left(\lambda + \frac{c}{2D_m}\right) \pm \sqrt{R(\lambda)}, \tag{3.27}$$

where

$$R(\lambda) = \frac{c^2}{4D_m^2} + c\lambda/D_m + 1/(D_m\tau_m). \tag{3.28}$$

Let us decompose λ into real and imaginary parts according to $\lambda = \alpha + i\beta$. Then

$$\omega_{\pm}(\lambda) = -u_{\pm}(\alpha,\beta) - iv_{\pm}(\alpha,\beta), \tag{3.29}$$

with

$$\frac{u_{\pm}(\alpha,\beta)}{c} = \alpha + \frac{c}{2D_m} \mp A(\alpha,\beta), \quad \frac{v_{\pm}(\alpha,\beta)}{c} = \beta \mp B(\alpha,\beta), \tag{3.30}$$

and (for $\beta > 0$)

$$A(\alpha,\beta) = \sqrt{\frac{1}{2}\left[R(\alpha) + \sqrt{R(\alpha)^2 + c^2\beta^2/D_m^2}\right]},$$

$$B(\alpha,\beta) = \sqrt{\frac{1}{2}\left[-R(\alpha) + \sqrt{R(\alpha)^2 + c^2\beta^2/D_m^2}\right]}. \tag{3.31}$$

One may now determine the linear stability of a solitary pulse by simultaneously solving $\mathrm{Re}[I(\lambda)] = \mathrm{Re}[I(0)] = 0$ and $\mathrm{Im}[I(\lambda)] = \mathrm{Im}[I(0)] = 0$ for α and β, with c determined by (3.22) (or equivalently (3.14) for the specific case of a rectangular pulse shape). This is illustrated in Fig. 3.5 for a rectangular pulse, which shows solutions with $\beta = 0$ and $\alpha < 0$ along the upper branch of Fig. 3.3. Moreover, α changes sign as it passes through the point where $d\rho_0/dc = 0$ in the (c, ρ_0) plane while moving from the upper solution branch to the lower. Hence, of the two possible traveling

wave solutions, the faster one is stable. Other solutions with $\alpha < 0$ and $\beta > 0$ are also found for both the fast and slow branches but do not affect the above stability argument.

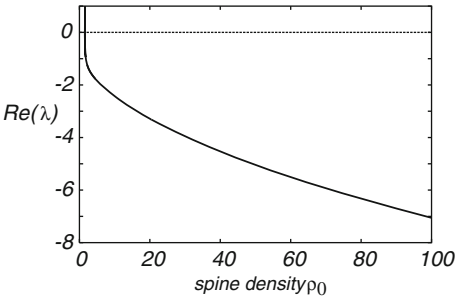

Fig. 3.5 A plot of the eigenvalues arising in the linearization of the SDS model shows that solutions with $\alpha < 0$ and $\beta = 0$ can be found for the branch of solutions with greatest speed. The graph above shows the behavior of $\alpha = \mathrm{Re}(\lambda)$ with $\beta = 0$ for the upper solution branch of Fig. 3.3. Note that $\alpha = 0$ at the point in the (c, ρ) plane at which the speed of the two possible traveling waves becomes equal. For the slower branch one finds that there exists solutions in the (α, β) plane with $\alpha > 0$ indicating that the slower branch is unstable

3.1.3 Discrete Distribution of Spines

So far we have assumed that the spine density is uniform. Although wave propagation failure is known to occur if the spine density is below some critical level, the numerical studies of Baer and Rinzel [19] suggest that propagation may be recovered by redistributing the spines into equally spaced dense clusters. Since interspine distances are of the order of μm and electronic length λ_m is typically measured in mm, we shall consider spine-head voltage at a cluster site to be the local spatial average of membrane potential in adjacent spines. Hence, we consider a discrete distribution of spines for which

$$\rho(x) = \bar{n} \sum_m \delta(x - x_m), \tag{3.32}$$

where x_m is the location of the mth spine cluster and $\bar{n}$ is the number of spines in a cluster. Such a distribution breaks continuous translation symmetry so that saltatory or lurching waves are expected rather than traveling waves of constant profile. (Saltatory waves are also found in myelinated axons; see Sect. 2.5.) We define a saltatory wave as an ordered sequence of firing times $\ldots T_{m-1} < T_m < T_{m+1}$ in which each spine cluster only fires once. Substituting the discrete density (3.32) into (3.1) with

$$\rho(x) a(x,t) = \bar{n} \sum_m \eta(t - T_m) \delta(x - x_m),$$

and making the approximation $\overline{n} \ll r_s$ so that the term $\rho(x)V/r_s$ can be neglected, we obtain the equation (using physical units)

$$\frac{\partial V}{\partial t} = -\frac{V}{\tau_m} + D_m \frac{\partial^2 V}{\partial x^2} + \frac{\bar{n}}{r_s} \sum_n \delta(x - x_n)\eta(t - T_n), \tag{3.33}$$

where we have absorbed a factor of r_m/τ_m into η and $D_m = \lambda_m^2/\tau_m$. This can be solved using the Green's functions G_0 of the cable equation:

$$V(x,t) = \frac{\overline{n}}{r_s} \sum_{m=0}^{\infty} H(x - x_m, t - T_m), \tag{3.34}$$

where we assumed the initial condition $V(x,0) = 0$ for all x.

$$H(x,t) = \int_0^t G_0(x,t-s)\eta(s)ds, \quad G_0(x,t) = \frac{1}{\sqrt{4\pi D_m t}} \mathrm{e}^{-t/\tau_m - x^2/4D_m t}. \tag{3.35}$$

Suppose that the spine clusters are uniformly distributed along the cable such that $x_m = md$, where d is the spacing between clusters. We will derive a condition for the existence of a saltatory wave solution given by $T_m = m\Delta$ for large m. The parameter Δ measures the time between successive threshold crossings at adjacent spine-head clusters such that the speed $c = d/\Delta$. First, using the causality condition $H(x,t) = 0$ for $t < 0$, it follows from (3.34) that

$$V(Nd, N\Delta) = \frac{\overline{n}}{r_s} \sum_{n=1}^{N} H(nd, n\Delta), \tag{3.36}$$

The wave speed of a saltatory wave (if it exists) is then determined self-consistently from the threshold condition

$$h = \lim_{N\to\infty} V(Nd, N\Delta) = \frac{\overline{n}}{r_s} \sum_{n=1}^{\infty} H(nd, n\Delta). \tag{3.37}$$

In order to calculate the wave speed, it is useful to rewrite (3.35) in the form

$$H(x,t) = \int_{-\infty}^{\infty} \frac{dk}{2\pi} \mathrm{e}^{ikx} \mathrm{e}^{-\varepsilon(k)t} \eta(k,t), \tag{3.38}$$

where $\eta(k,t) = \int_0^t \eta(s)\mathrm{e}^{\varepsilon(k)s} ds$. One may then exploit the convolution structure of (3.38) to evaluate it in closed form for a given $\eta(t)$. For the sake of illustration, consider again the rectangular pulse shape η, for which

$$\eta(k,t) = \eta_0(\mathrm{e}^{\varepsilon(k)\min(t,\tau_d)} - 1)/\varepsilon(k),$$

so that $H(x,t) = \eta_0[A(x,t - \min(t,\tau_d)) - A(x,t)]$, with

$$A(x,t) = \int_{-\infty}^{\infty} \frac{dk}{2\pi} \frac{\mathrm{e}^{ikx - \varepsilon(k)t}}{\varepsilon(k)}. \tag{3.39}$$

This is a standard integral given explicitly by

$$A(x,t) = \frac{1}{4}\sqrt{\frac{\tau_m}{D_m}}\left\{ e^{-|x|/\sqrt{\tau_m D_m}} \operatorname{erfc}\left(-\frac{|x|}{\sqrt{4D_m t}} + \sqrt{\frac{t}{\tau_m}} \right) + e^{|x|/\sqrt{\tau_m D_m}} \operatorname{erfc}\left(\frac{|x|}{\sqrt{4D_m t}} + \sqrt{\frac{t}{\tau_m}} \right) \right\}. \tag{3.40}$$

Finally, we may write the threshold condition in the form

$$h = \frac{\overline{n}}{r_s^2} \sum_{m=1}^{\infty} \hat{H}(md, m\Delta), \tag{3.41}$$

where $\hat{H}(x,t) = \eta_0[\hat{A}(x,t-\tau_d) - \hat{A}(x,t)]$, and

$$\hat{A}(x,t) = \int_{-\infty}^{0} e^{s/\hat{\tau}} A(x,t-s)ds. \tag{3.42}$$

The sum in (3.41) can then be performed numerically to obtain the speed of a saltatory wave $c = c(d,h)$.

In Fig. 3.6(a) we plot the speed c as a function of cluster spacing d for fixed threshold h, which shows that if the spine clusters are separated beyond some critical spacing, on the order of the electronic length $\lambda_m = 1$, a saltatory pulse will fail to propagate. Again linear stability analysis establishes that, as in the continuum model, it is the faster of the two branches that is stable. It is also instructive to consider the region in the (d,h) parameter plane where saltatory pulses exist. This may be obtained by continuing the limit point defining propagation failure of a saltatory pulse in the (d,c) plane as a function of h. The resulting phase diagram is shown in Fig. 3.6(b) and establishes that with increasing d the critical threshold for propagation failure decreases. Interestingly, the minimum wave speed of a stable saltatory pulse is found to be relatively insensitive to variation in cluster spacing d and threshold h. Now that the speed of a saltatory pulse has been determined as a function of system parameters it is possible to close the expression for the shape of a solitary pulse given by $V(x,t) = (\overline{n}/r_s)\sum_m H(x-md, t-md/v)$. A plot of this analytical expression is shown in Fig. 3.7, which clearly demonstrates that the saltatory pulse has a nonconstant profile.

Finally, note that there have been a number of recent extensions of the spike–diffuse–spike model. These include taking into account the branching structure of the dendritic tree [625], in which the Green's function G_0 is replaced by the Green's function of the tree, and incorporating active processes within the dendritic cable. In the latter case, each infinitesimal cable compartment is modeled as a quasi-linear LRC circuit, where the membrane resistance r_m is in series with an inductance L [624]; see Fig. 1.11. It should also be pointed out that from a mathematical perspective, the spike–diffuse–spike model is very similar in structure to the fire–diffuse–fire model of calcium puffs; see Sect. 4.3.

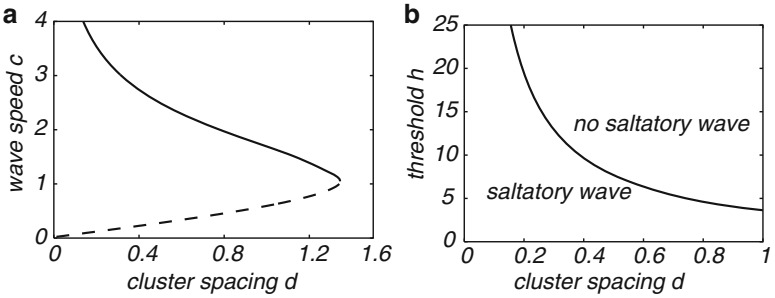

Fig. 3.6 (**a**) Plot of wave speed c for a saltatory pulse as a function of cluster spacing d. Here, $\hat{\tau} = \tau_d = 1$, $h = 2.5$, $r_s = 2$, $\eta_0 = 100$, and $\bar{n} = 2$. The upper (lower) branch is stable (unstable). (**b**) Continuation of the limit point in (**a**) showing the region in the (d,h)-plane where stable saltatory traveling waves exist

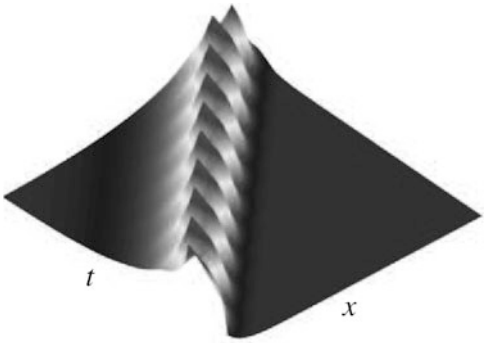

Fig. 3.7 Plot of the analytically obtained saltatory solution $V(x,t)$ in the dendritic cable with parameters as in Fig. 3.6 and $d = 1$. The x axis covers 10 lattice sites and the t axis $10d/c$

3.2 Reaction–Diffusion Model of CaMKII Translocation Waves

As we indicated at the beginning of this chapter, CaMKII (Ca^{2+}–calmodulin-dependent protein kinase II) is a key regulator of glutamatergic synapses and plays an essential role in many forms of synaptic plasticity. It has recently been observed experimentally that chemically stimulating a local region of dendrite not only induces the local translocation of CaMKII from the dendritic shaft to synaptic targets within spines, but also initiates a wave of CaMKII translocation that spreads distally through the dendrite with an average speed of order 1 μm/s [532]. In Fig. 3.8, we provide a cartoon of the mechanism for translocation waves hypothesized by Rose et al. [532]. Before local stimulation using a glutamate/glycine puff, the majority of CaMKII is in an inactive state and distributed uniformly throughout the dendrite. Upon stimulation, all CaMKII in the region of the puff (∼30 μm of dendrite) is converted to an active state, probably the autonomous state of CaMKII (see Fig. 3.8a), and begins translocating into spines. Simultaneously, a Ca^{2+} spike is

initiated and rapidly travels the length of the dendrite (as modeled in Sect. 3.1), causing CaMKII to bind Ca^{2+}/CaM along the way. In this primed or partially phosphorylated state, CaMKII does not yet translocate into spines. In the meantime, a portion of the activated CaMKII from the stimulated region diffuses into the region of primed CaMKII and the two types interact, with the result that primed CaMKII is activated. Some of these newly activated holoenzymes translocate into spines while others diffuse into more distal regions of the dendrite containing primed CaMKII, and the wave proceeds in this fashion. In certain cases one also finds a second wave propagating proximally from the stimulated site to the soma [532]. A schematic diagram illustrating the progression of a translocation wave along a dendrite following the rapid priming phase is shown in Fig. 3.8b.

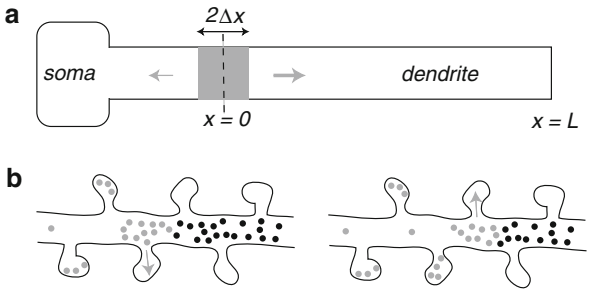

Fig. 3.8 Proposed mechanism of CaMKII translocation waves. (**a**) A glutamate/glycine puff activates CaMKII locally and initiates a fast Ca^{2+} spike that propagates distally (*indicated by larger horizontal arrow*) and primes CaMKII in the remainder of the dendrite. In certain cases one also finds a second wave propagating proximally from the stimulated site to the soma (*indicated by smaller horizontal arrow*). (**b**) Activated CaMKII (*gray dots*) both translocates into spines and diffuses into distal regions of the dendrite where it activates primed CaMKII (*black dots*). The net effect is a wave of translocated CaMKII propagating along the dendrite

A simple mathematical model of the above mechanism can be constructed using a system of reaction–diffusion equations for the concentrations of activated and primed CaMKII in the dendrite and spines [72, 161]. These equations incorporate three major components of the dynamics: *diffusion* of CaMKII along the dendrite, *activation* of primed CaMKII, and *translocation* of activated CaMKII from the dendrite to spines. For simplicity, consider a uniform one-dimensional, nonbranching dendritic cable as shown in Fig. 3.8a. Suppose that a region of width 30 μm is stimulated with a glutamate/glycine puff at time $t = 0$. The center of the stimulated region is taken to be at $x = 0$ and the distal end of the dendrite is at $x = L = 150\,\mu\text{m}$. The diffusion, activation, and translocation of CaMKII along the dendrite following stimulation are modeled according to the following system of equations:

$$\frac{\partial P}{\partial t} = D\frac{\partial^2 P}{\partial x^2} - k_0 AP \tag{3.43a}$$

$$\frac{\partial A}{\partial t} = D\frac{\partial^2 A}{\partial x^2} + k_0 AP - hA \tag{3.43b}$$

$$\frac{\partial S}{\partial t} = hA, \tag{3.43c}$$

where D is the diffusivity of CaMKII within the cytosol. Here $P(x,t)$ and $A(x,t)$ denote the concentration of primed and activated CaMKII at time $t > 0$ and location x along the dendrite. $S(x,t)$ denotes the corresponding concentration of CaMKII in the population of spines at the same time and distance. For simplicity, all parameters are constant in space and time. The reaction term kAP represents the conversion of CaMKII from its primed to active state based on the irreversible first-order reaction scheme

$$A + P \to 2A$$

with mass action kinetics, where k_0 is the rate at which primed CaMKII is activated per unit concentration of activated CaMKII. The decay term hA represents the loss of activated CaMKII from the dendrite due to translocation into a uniform distribution of spines at a rate h. The model assumes that translocation is irreversible over the time scale of simulations, which is reasonable given that activated CaMKII accumulation at synapses can persist for several minutes [569].

As a further simplification we will only consider the distal transport of CaMKII from the stimulated region by taking $0 \le x \le L$ and imposing closed or reflecting boundary conditions at the ends $x = 0, L$. Hence, no CaMKII can escape from the ends. In reality activated CaMKII could also diffuse in the proximal direction and trigger a second proximal translocation wave. However, the choice of boundary condition has little effect on the properties of the wave. Taking the distal half of the stimulated region to be $0 \le x \le 15\,\mu$m, consider the following initial conditions: $P(x,0) = 0$ and $A(x,0) = P_0$ for $0 \le x \le 15\,\mu$m, whereas $P(x,0) = P_0$ and $A(x,0) = 0$ for $x \ge 15\,\mu$m, where P_0 is the uniform resting concentration of CaMKII in the dendrite. Typical values of C range from 0.1 to 30μM [605], covering two orders of magnitude. We also set $S(x,0) = 0$ everywhere. In other words, we assume that all the CaMKII is activated within the stimulated region at $t = 0$, but none has yet translocated into spines nor diffused into the nonstimulated region. We also neglect any delays associated with priming CaMKII along the dendrite. This is a reasonable approximation, since the Ca^{2+} spike travels much faster than the CaMKII translocation wave [532]; see Sect. 3.1. Thus by the time a significant amount of activated CaMKII has diffused into nonstimulated regions of the dendrite, any CaMKII encountered there will already be primed. The benefit of this assumption is that it eliminates the need to model the Ca^{2+} spike. However, a more detailed model that takes into account the initial transient associated with the priming phase could be constructed by coupling the reaction–diffusion equations with the spike–diffuse–spike model of Sect. 3.1.

Note that the system of equations (3.43) is identical in form to the diffusive SI model introduced by Noble [464] to explain the spread of bubonic plague through Europe in the fourteenth century. In the latter model, $P(x,t)$ and $A(x,t)$ would rep-

resent the densities of susceptible and infective people at spatial location x at time t, respectively; k_0 would be the transmission rate and h the death rate. In the absence of translocation into spines ($h = 0$), the total amount of CaMKII is conserved so that $A(x,t) + P(x,t) = P_0$ for all x and $t \geq 0$. Equations (3.43) then reduce to the scalar Fisher–KPP equation

$$\frac{\partial A}{\partial t} = D\frac{\partial^2 A}{\partial x^2} + k_0 A(P_0 - A), \tag{3.44}$$

which was originally introduced to model the invasion of a gene into a population. The Fisher–KPP equation and its generalizations have been widely used to describe the spatial spread of invading species including plants, insects, genes, and diseases; see, for example, [285, 444, 575, 648] and references therein. One characteristic feature of such equations is that they support traveling fronts propagating into an unstable steady state, in which the wave speed and longtime asymptotics are determined by the dynamics in the leading edge of the wave—so-called pulled fronts [544]. In particular, a sufficiently localized initial perturbation (such as the stimulus used to generate CaMKII waves) will asymptotically approach the traveling front solution that has the minimum possible wave speed. (If we perform the change of variables $Q = P_0 - P$ in the CaMKII model, then the traveling wave solution constructed below propagates into the unstable state $A = 0, Q = 0$.) An overview of the theory of pulled fronts is presented in appendix section 3.3.

3.2.1 Translocation Waves for a Uniform Distribution of Spines

A traveling wave solution of (3.43a) and (3.43b) is $P(x,t) = P(\xi)$ and $A(x,t) = A(\xi)$, $\xi = x - ct$, where $c, c > 0$, is the wave speed, such that

$$P(\xi) \to P_0, \quad A(\xi) \to 0 \quad \text{as}\, \xi \to \infty$$

and

$$P(\xi) \to P_1 < P_0, \quad A(\xi) \to 0 \quad \text{as}\, \xi \to -\infty.$$

Here P_1 is the residual concentration of primed CaMKII following translocation of activated CaMKII into spines. The minimum wave speed can be calculated by substituting the traveling wave solution into (3.43a) and (3.43b) and linearizing near the leading edge of the wave where $P \to P_0$ and $A \to 0$. In the traveling wave coordinate frame (3.43a) and (3.43b) are transformed to

$$-c\frac{dP}{d\xi} = D\frac{d^2P}{d\xi^2} - k_0 AP \tag{3.45a}$$

$$-c\frac{dA}{d\xi} = D\frac{d^2A}{d\xi^2} + k_0 AP - hA \tag{3.45b}$$

This is a system of two second-order ordinary differential equations in the variable ξ. A global view of the nature of traveling wave solutions can be ob-

tained by identifying (3.45a) and (3.45b) with the equation of motion of a classical particle in two spatial dimensions undergoing damping due to "friction" and subject to an "external force." Thus we identify A and P with the "spatial" coordinates of the particle, ξ with the corresponding "time" coordinate, and the speed c as a "friction coefficient." If we ignore boundary effects by taking $-\infty < \xi < \infty$, then we can view a traveling wave solution as a particle trajectory that connects the point $(P,A) = (0,0)$ at $\xi = -\infty$ to the point $(P,A) = (P_0,0)$ at $\xi = \infty$. A restriction on the allowed values of c can now be obtained by investigating how the point $(1,0)$ is approached in the large-ξ limit.

Linearizing Eqs. (3.45a) and (3.45b) about the point $(P,A) = (P_0,0)$ we obtain a pair of second-order linear equations, which have solutions of the form $(P-P_0,A) = \mathbf{V}e^{-\lambda\xi}$ where λ and $\mathbf{V}$ satisfy the matrix equation

$$c\lambda\mathbf{V} = \begin{pmatrix} D\lambda^2 & -k \\ 0 & D\lambda^2 + k - h \end{pmatrix}\mathbf{V}, \tag{3.46}$$

where $k = k_0P_0$. Solving for the eigenvalue λ leads to the four solutions

$$\lambda = 0, \quad \frac{c}{D}, \quad \frac{c \pm \sqrt{c^2 - 4D(k-h)}}{2D} \tag{3.47}$$

and these, along with their corresponding eigenvectors $\mathbf{V}$, determine the shape of the wave as it approaches the point $(1,0)$. Note that the last two eigenvalues have a nonzero imaginary part when $c^2 < 4D(k-h)$, implying that as ξ becomes large the wave oscillates about the point $(1,0)$. This cannot be allowed since it would imply that the activated CaMKII concentration A takes on negative values (inspection of the corresponding eigenvectors shows that their components in the A-direction are nonzero and so A would indeed oscillate). Therefore, we must have

$$c \geq c_{\min} = 2\sqrt{D(k-h)}, \tag{3.48}$$

which implies that $k > h$. Note that the minimum wave speed can be identified with the linear spreading velocity of a pulled front; see appendix section 3.3. This then yields a more direct method for obtaining the minimum wave speed. That is, the characteristic equation obtained from (3.46) yields the dispersion relation

$$c(\lambda) = D\lambda + \frac{k-h}{\lambda}. \tag{3.49}$$

The theory of pulled fronts shows that the minimum wave speed is obtained by minimizing $c(\lambda)$. The equation $c'(\lambda) = 0$ gives $D\lambda = (k-h)/\lambda$, which has the solution $\lambda_0 = \sqrt{(k-h)/D}$, so that $c_{\min} = c(\lambda_0) = 2D\lambda_0 = 2\sqrt{D(k-h)}$.

An example of a numerically determined traveling wave solution with minimal speed $c_{\min}$ is shown in Fig. 3.9 for parameter values consistent with experimental studies of CaMKIIα, which is one of the two main isoforms of CaMKII. In its inactive state CaMKIIα tends to be located in the cytosol, whereas the other isoform, CaMKIIβ, is weakly actin bound [570]. One finds empirically that $D \sim 1\mu\text{m}^2/\text{s}$, $h \sim 0.05\,\text{s}^{-1}$ and $c \sim 1\,\mu\text{m/s}$ [532, 569, 570] for CaMKIIα. (CaMKIIβ has a diffusivity and translocation rate an order of magnitude smaller but exhibits compa-

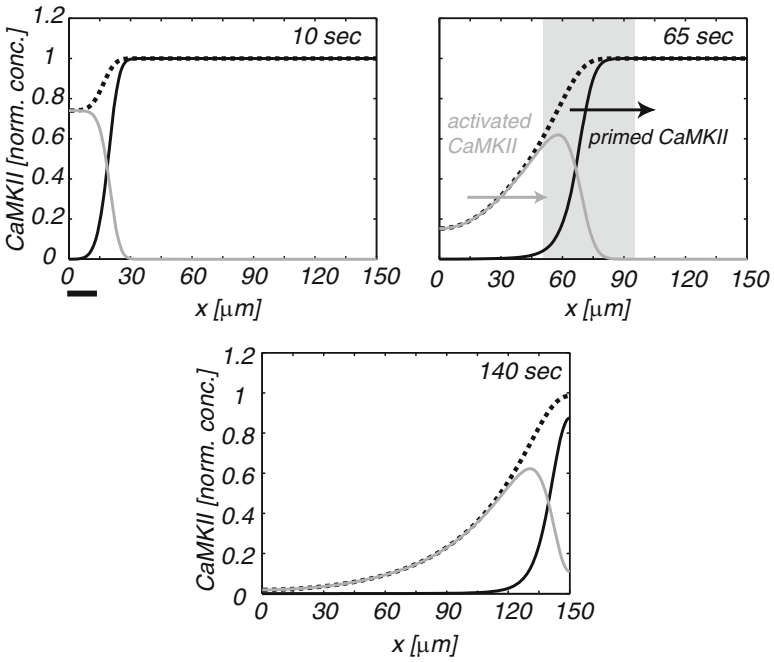

Fig. 3.9 Three successive snapshots of a numerically simulated translocation wave propagating along a homogeneous dendrite. Solutions of (3.43a) and (3.43b) are plotted for parameter values consistent with experimental data on CaMKII [532, 569, 570]. The translocation rate $h = 0.05\,\mathrm{s}$, diffusivity $D = 1\,\mu\mathrm{m}^2/\mathrm{s}$ and the activation rate $k_0 P_0 = 0.21\,\mathrm{s}$. At time $t = 0$ all of the CaMKII within the stimulated region (*indicated by thick bar*) is in the activated state, whereas all of the CaMKII within the nonstimulated region is in the primed state. Concentrations are normalized with respect to the initial concentration of primed CaMKII. Composite wave consists of a pulse of activated CaMKII (*gray curve*) moving at the same speed as a front of primed CaMKII (*black curve*). Also shown is the total CaMKII concentration along the dendrite (*dashed black curve*), which decreases with time due to translocation into spines. As indicated in the center plot, the front forms an interface between a quiescent region containing a uniform concentration of primed CaMKII and a region dominated by translocation of activated CaMKII into spines. The dynamics in the interfacial (*shaded*) region is dominated by diffusion–activation of primed CaMKII

rable wave speeds.) The formula for the wave speed then gives an estimate for the unknown activation rate, $k \sim 0.2\,\mathrm{s}^{-1}$. It can be seen in Fig. 3.9 that the wave profile of primed CaMKII is in the form of a front, whereas the co-moving wave profile of activated CaMKII is a localized pulse.

The above analysis predicts wave propagation failure when the translocation rate h is greater than the effective activation rate k. Experimentally, h is determined by globally activating CaMKII along a dendrite and determining the rate at which the level of CaMKII decays [569, 570]. The detailed microscopic mechanism whereby CaMKII is translocated into spines is currently not known, so it is difficult to relate h to individual spine properties. A simple hypothesis is that the translocation rate depends on the spine density according to $h = \rho_0 v_0$, where v_0 is an effective "velocity" associated with translocation into an individual spine. Since the activa-

tion rate $k = k_0 P_0$, where P_0 is the initial concentration of primed CaMKII in the nonstimulated region of the dendrite, the model predicts that CaMKII translocation waves will fail to propagate when

$$\rho_0 v_0 > k_0 P_0. \tag{3.50}$$

For example, this inequality predicts that dendrites with a high density of spines are less likely to exhibit translocation waves than those with a low spine density. It also predicts that dendrites with a larger initial concentration of primed CaMKII in the shaft are more likely to exhibit translocation waves than those with a smaller initial concentration. Since the initial concentration P_0 of primed CaMKII depends on the effectiveness of the Ca^{2+} spike in both propagating along the dendrite and priming the inactive state, the model agrees with the experimental finding that translocation waves fail to propagate when L-type Ca^{2+} channels are blocked [532]. One also finds that Ca^{2+} spikes are less likely to propagate towards the soma, which could explain why translocation waves are more often observed propagating towards the distal end of a dendrite.

3.2.2 *Pulsating Waves in the Presence of Discretely Distributed Spines*

One of the major simplifications of the above model is that the discrete nature of dendritic spines is ignored by treating the spine density ρ and, hence, the translocation rate h as uniform. Given the fact that the radius of the spine neck is typically at the submicron level, which is much smaller than any other length scale of the system, one can take into account the discreteness of spines by representing the spine density as the sum of Dirac delta functions (3.32), which represents clusters of $\bar{n}$ spines at discrete locations x_n; see Sect. 3.1. It immediately follows that the translocation rate h is itself space-dependent and (3.43a) and (3.43b) become heterogeneous. For the sake of illustration, consider the case of a set of spine clusters that are uniformly spaced with $x_n = n\Delta$ where Δ is the spine cluster spacing. In order to separate the effects of discreteness from the effects of spine density, we will assume that the size of a cluster scales with Δ so that $\bar{n} = \rho_0 \Delta$ with ρ_0 fixed. Thus, setting $\bar{h} = \rho_0 v_0$, we have the space-dependent translocation rate

$$h(x) = \bar{h}\Delta \sum_{n\in\mathbb{Z}} \delta(x - n\Delta), \tag{3.51}$$

such that $L^{-1}\int_0^L h(x)dx = \bar{h}$ for $L \gg \Delta$.

In recent years, there has been an increasing interest in studying biological invasion in heterogeneous environments using reaction–diffusion equations [40, 102, 212, 335, 574, 575, 587, 664, 687]. Heterogeneity is often incorporated by assuming that the diffusion coefficient and the growth rate of a population are periodically varying functions of space. One of the simplest examples of a single population model in a periodic environment was proposed by Shigesada et al.

[574, 575], in which two different homogeneous patches are arranged alternately in one-dimensional space so that the diffusion coefficient and the growth rate are given by periodic step functions. The authors showed numerically that an invading population starting from a localized perturbation evolves to a traveling periodic wave in the form of a pulsating front. The population density $u(x,t)$ of such a wave is defined by the condition $u(x,t) = u(x+\sigma, t+T)$ such that $\lim_{x\to\infty} u(x,t) = 0$ and $\lim_{x\to-\infty} u(x,t) = p(x)$, where $p(x)$ is a spatially periodic stationary solution of the corresponding reaction–diffusion equation. This form of solution repeats itself in a time interval T if it is observed at two successive points separated by a distance σ. The speed of the wave is then taken to be $c = \sigma/T$. Shigesada et al. [574] also used linearized information within the leading edge of the pulsating front to derive wave speed estimates, generalizing the analysis of pulled fronts in homogeneous media [544]. An interesting recent extension of this approach has been used to study pulsating fronts in periodically modulated nonlocal neural field equations [132]. The theory of pulsating fronts has also been developed in a more general and rigorous setting [40, 212, 587, 664, 687].

The analysis of CaMKII translocation waves developed in [72] follows the basic formulation of Shigesada et. al. [574] by linearizing (3.43b) at the leading edge of the wave where $A(x,t) \to 0$ and $\mathscr{P}(x,t) \to P_0$:

$$\frac{\partial A}{\partial t} = D\frac{\partial^2 A}{\partial x^2} + kA - h(x)A, \tag{3.52}$$

with $h(x)$ given by the Δ-periodic function (3.51). Assume a solution of the form $A(x,t) = a(\xi)\mathscr{P}(x)$, $\xi = x - ct$, and set

$$\frac{\partial}{\partial t} \to -c\frac{\partial}{\partial \xi}, \quad \frac{\partial}{\partial x} \to \frac{\partial}{\partial x} + \frac{\partial}{\partial \xi}.$$

Substitution into (3.52) then gives

$$-c\mathscr{P}(x)a'(\xi) = D\left[a''(\xi)\mathscr{P}(x) + 2a'(\xi)\mathscr{P}'(x) + a(\xi)\mathscr{P}''(x)\right] + [k - h(x)]a(\xi)\mathscr{P}(x).$$

Dividing through by $a(\xi)\mathscr{P}(x)$ and rearranging yields

$$D\frac{a''(\xi)}{a(\xi)} + \left[2D\frac{\mathscr{P}'(x)}{\mathscr{P}(x)} + c\right]\frac{a'(\xi)}{a(\xi)} = -D\frac{\mathscr{P}''(x)}{\mathscr{P}(x)} - k + h(x). \tag{3.53}$$

Applying the operator $\partial_x\partial_\xi$ to both sides of (3.53) implies that either $\mathscr{P}'(x)/\mathscr{P}(x)$ is a constant or $a'(\xi)/a(\xi)$ is a constant. Only the latter condition is consistent with $P(x)$ being a periodic function. Thus, $a(\xi) = A_0 e^{-\lambda\xi}$ with λ determined by solutions to the damped Hill equation

$$\mathscr{P}''(x) - 2\lambda\mathscr{P}'(x) + \left[\lambda^2 + \frac{k - h(x) - c\lambda}{D}\right]\mathscr{P}(x) = 0. \tag{3.54}$$

Note that if $\mathscr{P}(x) = e^{\lambda x}U(x)$ then $U(x)$ satisfies the undamped Hill equation

$$DU''(x) + [k - h(x) - c\lambda]\, U(x) = 0. \tag{3.55}$$

In order to determine the minimal wave speed $c_{\min}$, it is necessary to find a bounded periodic solution $P(x)$ of (3.54), which yields a corresponding dispersion relation $c = c(\lambda)$, whose minimum with respect to λ can then be determined (assuming it exists). Unfortunately, for general periodic functions $h(x)$, it is not possible to solve (3.54) explicitly, and some form of approximation scheme is required as described in the next section.

3.2.3 Homogenization of Pulsating Waves for a Fast Periodic Modulation of Spine Density

Since the spine cluster spacing Δ is at least an order of magnitude smaller than the width of the traveling wave of the homogeneous system, one can use homogenization theory to approximate the discrete effects of spines by a corresponding continuum model [72]. Such a method has also been applied to studying variations in electrical voltage/conductance [424] and the distribution of protein receptors [68] along spiny dendrites. Interestingly, Smaily et al. [587] independently applied the same homogenization procedure to analyze wave speed in the population model of Shigesada et. al. [574]. A more general discussion of homogenization techniques applied to traveling fronts can be found in the review by Xin [687].

As a first step, we introduce a macroscopic length scale σ and set $\Delta = \varepsilon\sigma$ with $\varepsilon \ll 1$. We identify σ with the effective width of the primed CaMKII front, which turns out to be around 20–30 μm in the given parameter regimes. Equation (3.55) can then be rewritten in the form

$$\frac{d^2U}{dx^2} + \left[\overline{\Gamma} - \Delta\Gamma\left(\frac{x}{\varepsilon}\right)\right] U(x) = 0, \tag{3.56}$$

where

$$\overline{\Gamma} = [k - c\lambda - \overline{h}]/D \tag{3.57}$$

and

$$\Delta\Gamma(y) = \frac{\overline{h}}{D}\left(\sigma \sum_{n\in\mathbb{Z}} \delta(y - n\sigma) - 1\right) \tag{3.58}$$

such that $\Delta\Gamma(y)$ is a σ-periodic function of y. Applying the homogenization procedure outlined below leads to the result

$$U(x) = \langle U(x)\rangle \left[1 + \varepsilon^2 \Delta U(x/\varepsilon)\right] + \mathcal{O}(\varepsilon^3), \tag{3.59}$$

where $\langle U \rangle$ satisfies the averaged equation

$$\frac{d^2\langle U\rangle}{dx^2} + \Gamma_\varepsilon \langle U\rangle = 0, \tag{3.60}$$

and

$$\Gamma_\varepsilon = \overline{\Gamma} - \varepsilon^2 \Gamma_2 + \mathscr{O}(\varepsilon^3), \quad \Gamma_2 = \frac{1}{12}\left(\frac{\overline{h}\sigma}{D}\right)^2, \tag{3.61}$$

$$\Delta U(y) = \frac{\overline{h}\sigma^2}{D}\left[\frac{y}{2\sigma} - \frac{y^2}{2\sigma^2} - \frac{1}{12}\right]. \tag{3.62}$$

Homogenization method for discrete spines. The basic idea of multi-scale homogenization is to expand the solution of Eq. (3.56) as a power series in ε, with each term in the expansion depending explicitly on the "slow" (macroscopic) variable x and the "fast" (microscopic) variable $y = x/\varepsilon$ [68, 424, 587]:

$$U(x,y) = U_0(x) + \varepsilon U_1(x,y) + \varepsilon^2 U_2(x,y) + \ldots, \tag{3.63}$$

where $U_j(x,y), j = 1,\ldots$ are σ-periodic in y. The perturbation series expansion is then substituted into Eq. (3.56) with x, y treated as independent variables so that derivatives with respect to x are modified according to $\partial_x \to \partial_x + \varepsilon^{-1}\partial_y$. This generates a hierarchy of equations corresponding to successive powers of ε:

$$\frac{\partial^2 U_1}{\partial y^2} = 0 \tag{3.64}$$

$$\frac{d^2 U_0}{dx^2} + 2\frac{\partial^2 U_1}{\partial x \partial y} + \frac{\partial^2 U_2}{\partial y^2} + \left[\overline{\Gamma} - \Delta\Gamma(y)\right] U_0 = 0 \tag{3.65}$$

at powers $\varepsilon^{-1}, 1$ and

$$\frac{\partial^2 U_n}{\partial x^2} + 2\frac{\partial^2 U_{n+1}}{\partial x \partial y} + \frac{\partial^2 U_{n+2}}{\partial y^2} + \left[\overline{\Gamma} - \Delta\Gamma(y)\right] U_n = 0 \tag{3.66}$$

at $\mathscr{O}(\varepsilon^n), n \geq 1$.

Equation (3.64) and boundedness of U_1 imply that U_1 is independent of y and can thus be absorbed into $U_0(x)$. Thus the leading-order corrections arising from small-scale fluctuations in the spine density occur at $\mathscr{O}(\varepsilon^2)$. Define the spatial average of a periodic function $F(y)$, denoted by $\langle F \rangle$, according to

$$\langle F \rangle = \frac{1}{\sigma}\int_0^\sigma F(y)dy. \tag{3.67}$$

Taking the spatial average of (3.65) with $U_0 = \langle U_0 \rangle$ then gives

$$\frac{d^2 U_0}{dx^2} + \overline{\Gamma} U_0 = 0. \tag{3.68}$$

We have exploited the fact that U_2 is periodic in y so $\langle \partial^2 U_2/\partial y^2 \rangle = 0$. In order to calculate U_2, we first subtract the averaged Eq. (3.68) from (3.65) to obtain

$$\frac{\partial^2 U_2}{\partial y^2} = \Delta\Gamma(y) U_0(x). \tag{3.69}$$

It follows that $U_2(x,y) = U_0(x)\chi(y)$ with $\chi''(y) = \Delta\Gamma(y)$ and χ a σ-periodic function of y. Integrating once with respect to y gives $\chi'(y) = \chi'(0) + \int_0^y \Delta\Gamma(z)dz$. We can eliminate the unknown $\chi'(0)$ by spatially averaging with respect to y and using $\langle\chi'\rangle = 0$. This gives $\chi'(y) = \oint_0^y \Delta\Gamma(z)dz$ with

$$\oint_0^y f(z)dz \equiv \int_0^y f(z)dz - \left\langle \int_0^y f(z)dz \right\rangle \tag{3.70}$$

for any integrable function f. Another integration with respect to y shows that

$$\chi(y) = \chi(0) + \int_0^y \oint_0^{y'} \Delta\Gamma(z)dzdy'.$$

Spatially averaging this equation with respect to y in order to express $\chi(0)$ in terms of $\langle\chi\rangle$ and multiplying through by $U_0(x)$ finally gives

$$\begin{aligned} \Delta U_2(x,y) &\equiv U_2(x,y) - \langle U_2\rangle(x) \\ &= U_0(x) \oint_0^y \oint_0^{y'} \Delta\Gamma(z)dzdy'. \end{aligned} \tag{3.71}$$

It remains to determine the equation satisfied by $\langle U_2\rangle$. Spatially averaging Eq. 3.66) for $n = 2$ gives

$$\frac{d^2\langle U_2\rangle}{dx^2} + \overline{\Gamma}\langle U_2\rangle = \langle \Delta\Gamma(y)U_2(x,y)\rangle. \tag{3.72}$$

Substituting (3.71) into (3.72) and reordering the resulting multiple integral yields the result

$$\frac{d^2\langle U_2\rangle}{dx^2} + \overline{\Gamma}\langle U_2\rangle = -\left\langle \left(\oint_0^y \Delta\Gamma(z)dz \right)^2 \right\rangle U_0(x). \tag{3.73}$$

Finally, writing $\langle U\rangle = U_0 + \varepsilon^2\langle U_2\rangle + \ldots$ we obtain the homogenized version of the Hill equation (3.55):

$$\frac{d^2\langle U\rangle}{dx^2} + \Gamma_\varepsilon\langle U\rangle = 0, \tag{3.74}$$

where

$$\Gamma_\varepsilon = \overline{\Gamma} + \varepsilon^2\Gamma_2 + \mathcal{O}(\varepsilon^3), \quad \Gamma_2 = \left\langle \left(\oint_0^y \Delta\Gamma(z)dz \right)^2 \right\rangle. \tag{3.75}$$

It is straightforward to calculate the integrals in (3.71) and (3.75) for a periodic spine density with $\Delta\Gamma(y)$ given by (3.58) [424]:

$$\Gamma_2 = \left\langle \left(\oint_0^y \Delta\Gamma(z)dz \right)^2 \right\rangle = \frac{1}{12}\left(\frac{\overline{h}\sigma}{D} \right)^2, \tag{3.76}$$

$$\oint_0^y \oint_0^{y'} \Delta\Gamma(z)dzdy' = \frac{\overline{h}\sigma^2}{D}\left[\frac{y}{2\sigma} - \frac{y^2}{2\sigma^2} - \frac{1}{12} \right]. \tag{3.77}$$

We thus obtain (3.59) and (3.60).

Note that it is possible to extend the above homogenization scheme to the case of randomly rather than periodically distributed spines, provided that the resulting heterogeneous medium is *ergodic*. That is, the result of averaging over all realizations of the ensemble of spine distributions is equivalent to averaging over the length L of the dendrite in the infinite-

L limit. If such an ergodic hypothesis holds and L is sufficiently large so that boundary terms can be neglected, then the above analysis carries over with $\langle\cdot\rangle$ now denoting ensemble averaging [424].

Recall from our discussion of (3.54) that the solution $\mathscr{P}(x) = e^{\lambda x}U(x)$ has to be a bounded Δ-periodic function of x. It follows from (3.59) and (3.60) that $e^{\lambda x}\langle U(x)\rangle$ should be a finite constant. Writing the solution of (3.60) as $\langle U(x)\rangle \sim e^{-\sqrt{-\Gamma_2}\varepsilon x}$, yields the characteristic equation

$$\lambda = \sqrt{\frac{c\lambda - k + \overline{h}}{D} - \varepsilon^2\Gamma_2}, \tag{3.78}$$

where we have substituted for $\overline{\Gamma}$ using (3.57). Squaring both sides and rearranging thus leads to the following dispersion relation for the wave speed c:

$$c = c(\lambda) \equiv D\lambda + \frac{k - \overline{h} + \varepsilon^2 D\Gamma_2}{\lambda}. \tag{3.79}$$

Minimizing with respect λ then shows that

$$c_{\min} = 2\sqrt{D(k-\overline{h}) + \varepsilon^2 D^2\Gamma_2}, \tag{3.80}$$

For sufficiently small ε, we can Taylor expand (3.80) to obtain

$$c_{\min} \approx \overline{c} + \frac{2D^2\Gamma_2}{\overline{c}}\varepsilon^2, \tag{3.81}$$

with $\overline{c} = 2\sqrt{D(k-\overline{h})}$ the wave speed of the corresponding homogeneous distribution of spines. Hence, a periodic variation in the spine density due to clustering leads to an $\mathscr{O}(\varepsilon^2)$ increase in the wave speed. An analogous result was obtained by Smaily et. al. [587] for the Shigesada et. al. model [574]. Note that (3.59) also implies that there are small-scale fluctuations of the wave profile in the leading edge of the wave

$$\frac{\Delta P(x/\varepsilon)}{\langle P\rangle} = \varepsilon^2 \Delta U(x/\varepsilon) + \mathscr{O}(\varepsilon^3). \tag{3.82}$$

Since $\varepsilon = \Delta/\sigma$, it follows from (3.62) that fluctuations in the wave profile vary between $-\overline{h}\Delta^2/(12D)$ at spine clusters and $\overline{h}\Delta^2/(24D)$ between spine clusters. In terms of physical parameters, the minimum wave speed is

$$c_{\min} = 2\sqrt{D(k-\overline{h}) + \Delta^2\overline{h}^2/12}. \tag{3.83}$$

It immediately follows that for fixed $\overline{h}, k, D$ (and hence $\overline{c}$), spine clustering increases the speed of a translocation wave. This is illustrated in Fig. 3.10, where we plot the minimal wave speed $c_{\min}$ given by (3.83) as a function of the activation rate k for various values of the cluster spacing Δ. An additional important consequence of clustering is that it reduces the threshold for the existence of a translocation wave.

That is, there exists a critical value of the activation rate, $k = \kappa(\Delta)$, below which translocation waves do not exist and $\kappa(\Delta)$ is a decreasing function of Δ. In the homogenization limit $\Delta \to 0$, we recover the result $\kappa = \bar{h}$.

The existence of a pulsating wave due to spine clustering and the associated increase (decrease) in the minimal speed (threshold) of the wave can also be confirmed numerically. For the sake of illustration, consider a dendrite of length $L = 300\,\mu\text{m}$ with reflecting boundary conditions at both ends $x = 0, L$. The initial conditions are taken to be

$$\begin{aligned} P(x,0) &= P_0, A(x,0) = 0 \text{ for all} x \notin [0, \delta L] \\ P(x,0) &= 0, A(x,0) = P_0 \text{ for all} x \in [0, \delta L], \end{aligned}$$

with $\delta L = 15\,\mu\text{m}$. We discretize space by setting $x = m\delta x$, where δx is the step length and $m = 0, 1, \ldots, M$ with $M = L/\delta x$. In discrete spatial units the spine cluster spacing is taken to be $\Delta = P\delta x$. The spine cluster distribution is then represented numerically by the discrete sum

$$\rho(m\delta x) = \frac{1}{\delta x} \sum_{j=0}^{M/P} \delta_{m,jP},$$

where $\delta_{m,j}$ is the Kronecker delta and δx is chosen so that M, P and M/P are integers. An example of a pulsating wave is shown in Fig. 3.11. Comparison between waves for a spatially uniform distribution of spines and a spatially discrete distribution of spine clusters shows that the wave is periodically modulated and faster in the latter case. This is a consequence of the fact that translocation is less effective

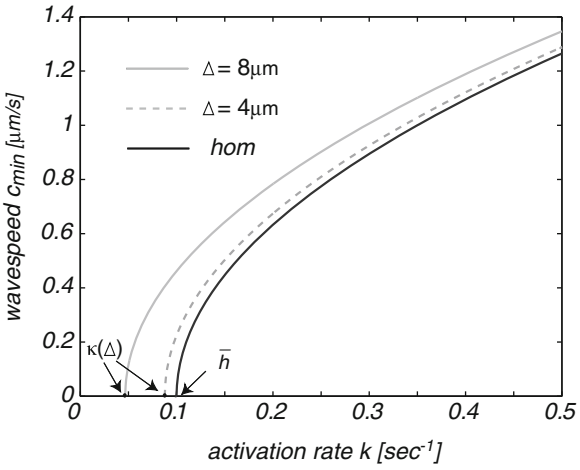

Fig. 3.10 Plot of minimal wave speed $c_{\min}$ as a function of activation rate $k = k_0 P_0$ for various values of the spine cluster spacing Δ. Also shown is the corresponding wave speed for a homogeneous spine distribution (*black curve*). Other parameters are $\bar{h} = 0.1\,\text{s}^{-1}$ and $D = 1\,\mu\text{m}^2/\text{s}$. Note that wave propagation failure occurs as $k \to \kappa(\Delta)$ from above where $\kappa(\Delta)$ is the propagation threshold

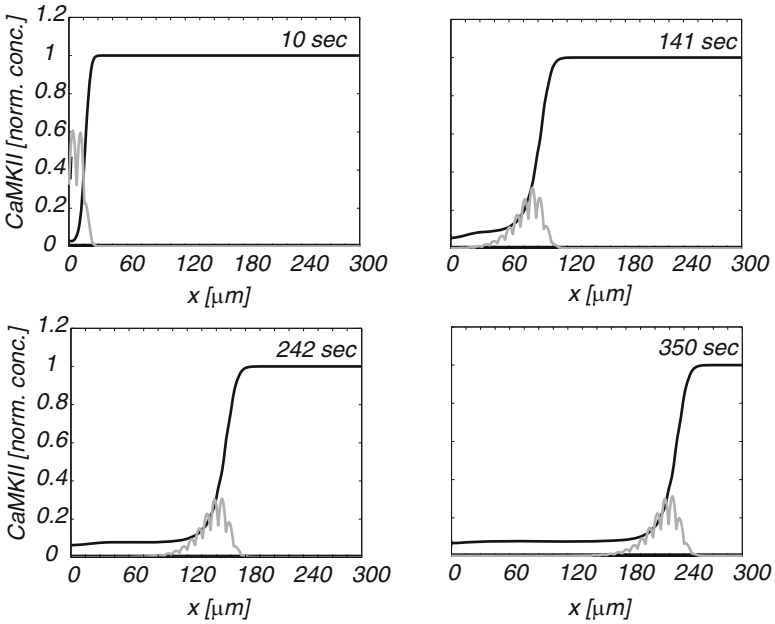

Fig. 3.11 Numerical traveling wave solution of (3.43a) and (3.43b) for an inhomogeneous distribution of spine clusters with $\Delta = 8\,\mu$m. The translocation rate $\overline{h} = 0.1$ s, diffusivity $D = 1\,\mu\text{m}^2/\text{s}$ and the activation rate $k = 0.19$ s. At time $t = 0$ all of the CaMKII within the stimulated region (*indicated by thick bar*) is in the activated state, whereas all of the CaMKII within the nonstimulated region is in the primed state. Concentrations are normalized with respect to the initial concentration of primed CaMKII. The resulting wave profiles for activated (*gray curve*) and primed (*black curve*) CaMKII along the dendrite are shown at four successive snapshots in time. The numerically estimated wave speed $c_{\min} \approx 0.66\,\mu$m/s, which is faster than the wave speed $\overline{c} = 0.6\,\mu$m/s of the corresponding uniform spine distribution

in the presence of spine clusters. Although doubling the degree of clustering only leads to a change in wave speed of order 0.05μm/s (consistent with the analytical calculations), it leads to a significant difference in propagation times along a 300 μm dendrite.

3.2.4 Wave Speed for a Slowly Modulated Spine Density

So far we have considered the effects of heterogeneity at a microscopic length scale comparable to the spacing of individual spines. In particular, we took the homogenized translocation rate $\overline{h}$ to be constant over the length of a dendrite. However, it is found experimentally that there is a slow proximal to distal variation in the density of spines [22, 346]. An illustration of a typical spine density found in pyramidal neurons of mouse cortex [22] is shown in Fig. 3.12. Such a variation in spine

density can be incorporated into (3.43a) and (3.43b) by setting $h = \overline{h} + \Delta h(\varepsilon x)$, where $\overline{h}$ denotes the translocation rate at the initiation point x_0 of the wave and $\Delta h(\varepsilon x)$ represents the slow modulation of the (homogenized) translocation rate over the length of a dendrite with $\varepsilon \ll 1$. The general problem of biological invasion in slowly modulated heterogeneous environments can be analyzed using a Hamilton–Jacobi method for front velocity selection [421, 687]; see Sect. 3.3. This method was originally applied to homogeneous media by Freidlin using large deviation theory [203, 204, 212] and was subsequently formulated in terms of PDEs by Evans and Sougandis [178]. We will illustrate the method by applying it to the reaction–diffusion model of CaMKII translocation waves with slow periodic modulation; see also [72]

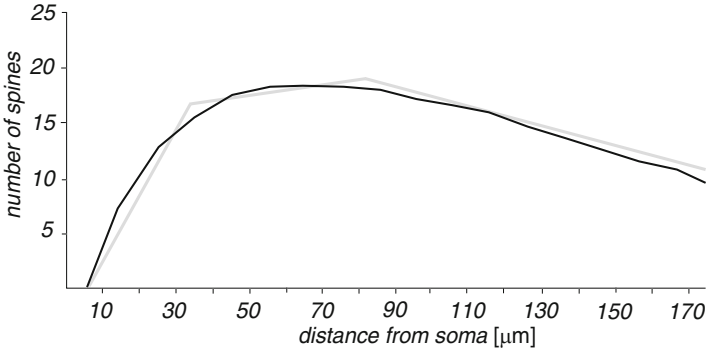

Fig. 3.12 Illustrative example of the spine density variation along the basal dendrite of a pyramidal cell in mouse cortex (*black curve*). Density is calculated as the number of spines per 10 μm segment of the dendrite from the soma to the tip of the dendrite. Abstracted from experimental data in [22]. Also shown is a simplified piecewise linear approximation of the spine density variation (*gray curve*)

The first step in the analysis is to rescale space and time in (3.43a) and (3.43b) according to $t \to t/\varepsilon$ and $x \to x/\varepsilon$; see [178, 204, 421]:

$$\varepsilon \frac{\partial P}{\partial t} = D\varepsilon^2 \frac{\partial^2 P}{\partial x^2} - k_0 AP \tag{3.84a}$$

$$\varepsilon \frac{\partial A}{\partial t} = D\varepsilon^2 \frac{\partial^2 A}{\partial x^2} + k_0 AP - [\overline{h} + \Delta h(x)]A. \tag{3.84b}$$

Under the spatial rescaling the front region where A (P) rapidly increases (decreases) as x decreases from infinity becomes a step as $\varepsilon \to 0$. This motivates the introduction of solutions of the form

$$P(x,t) \sim P_0 \left[1 - \mathrm{e}^{-G_\varepsilon(x,t)/\varepsilon}\right], \quad A(x,t) \sim A_0(x)\mathrm{e}^{-G_\varepsilon(x,t)/\varepsilon} \tag{3.85}$$

with $G_\varepsilon(x,t) > 0$ for all $x > x(t)$ and $G_\varepsilon(x(t),t) = 0$. The point $x(t)$ determines the location of the front and $c = \dot{x}$. Substituting (3.85) into (3.84a) and (3.84b) gives

$$-\frac{\partial G_\varepsilon}{\partial t} = D\left[\frac{\partial G_\varepsilon}{\partial x}\right]^2 - D\varepsilon\frac{\partial^2 G_\varepsilon}{\partial x^2} - k_0 A_0(x)\left[1-\mathrm{e}^{-G_\varepsilon(x,t)/\varepsilon}\right]$$

$$-A_0(x)\frac{\partial G_\varepsilon}{\partial t} = A_0(x)\left[D\left[\frac{\partial G_\varepsilon}{\partial x}\right]^2 - D\varepsilon\frac{\partial^2 G_\varepsilon}{\partial x^2} + k_0 P_0\left[1-\mathrm{e}^{-G_\varepsilon(x,t)/\varepsilon}\right] - [\overline{h}+\Delta h(x)]\right]$$
$$+\varepsilon^2 A_0''(x)G_\varepsilon - 2\varepsilon A_0'(x)\frac{\partial G_\varepsilon}{\partial x}.$$

Since $\mathrm{e}^{-G_\varepsilon(x,t)/\varepsilon} \to 0$ as $\varepsilon \to 0$ for $G_\varepsilon > 0$, it follows that the limiting function $G(x,t) = \lim_{\varepsilon\to 0} G_\varepsilon(x,t)$ satisfies

$$-\frac{\partial G}{\partial t} = D\left[\frac{\partial G}{\partial x}\right]^2 - k_0 A_0(x) \tag{3.86a}$$

$$-\frac{\partial G}{\partial t} = D\left[\frac{\partial G}{\partial x}\right]^2 + k - [\overline{h}+\Delta h(x)], \tag{3.86b}$$

where $k = k_o P_0$ as before. It immediately follows that

$$A_0(x) = \left[\frac{k-\overline{h}-\Delta h(x)}{k}\right] P_0. \tag{3.87}$$

The remaining equation (3.86b) can be analyzed along identical lines to a previous study of the heterogeneous Fisher–KPP equation [421]. Formally comparing (3.86b) with the Hamilton–Jacobi equation $\partial_t G + H(\partial_x G, x) = 0$, we define the Hamiltonian

$$H = Dp^2 + k - [\overline{h}+\Delta h(x)], \tag{3.88}$$

where $p = \partial_x G$ is interpreted as the conjugate momentum of x. It now follows that (3.86b) can be solved in terms of the Hamilton equations

$$\frac{dx}{ds} = 2Dp, \quad \frac{dp}{ds} = \frac{d\Delta h}{dx}. \tag{3.89}$$

Combining these equations yields the second-order ODE

$$\ddot{x} - 2D\Delta h(x)' = 0. \tag{3.90}$$

This takes the form of a Newtonian particle moving in a "potential" $V(x) = -2D\Delta h(x)$. Given the solution $x(s) = \phi(s;x,t)$ with $\phi(0;x,t) = x_0$ and $\phi(t;x,t) = x$, we can then determine $G(x,t)$ according to

$$G(x,t) = -E(x,t)t + \frac{1}{2D}\int_0^t \dot{\phi}(s;x,t)^2 ds. \tag{3.91}$$

Here

$$E(x,t) = H(\dot{\phi}(s;x,t)/2D, \phi(s;x,t)), \tag{3.92}$$

which is independent of s due to conservation of energy.

For certain choices of the modulation function $\Delta h(x)$, (3.90) can be solved explicitly [421]. In particular, suppose that the spine density curve in Fig. 3.3 is approximated by a piecewise linear function, in which the density increases linearly with distance from the soma to some intermediate location κ along the dendrite and then decreases linearly towards the distal end. Assuming that the right-moving wave is initiated beyond the point κ, $x_0 > \kappa$, then we can simply take $\Delta h(x) = -\beta(x - x_0)$ for $\beta > 0$. Substituting into (3.90) and integrating twice with respect to s using the Cauchy conditions gives

$$\phi(s;x,t) = x_0 + (x - x_0)s/t + D\beta ts - D\beta s^2. \tag{3.93}$$

The corresponding "energy" function is then

$$E(x,t) = \frac{(x - x_0)^2}{4Dt^2} + k - \overline{h} + \frac{\beta}{2}(x - x_0) + \frac{\beta^2}{4}Dt^2 \tag{3.94}$$

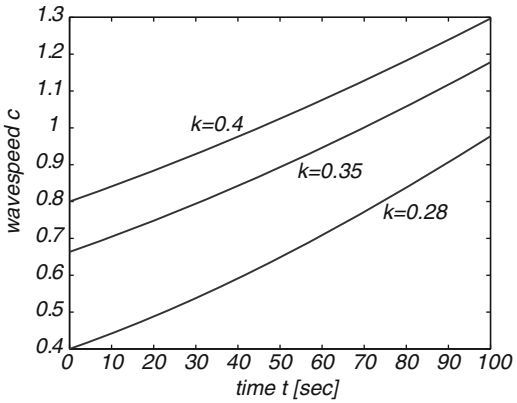

Fig. 3.13 Plot of time-dependent variation in wave speed c given by (3.96) for various values of the activation rate k. Other parameters are $\overline{h} = 0.24\,\mathrm{s}^{-1}$ and $D = 1\,\mu\mathrm{m}^2/\mathrm{s}$. At $t = 0$, $c(0) = 2\sqrt{D(k - \overline{h})}$

and (3.91) shows that

$$G(x,t) = \frac{(x - x_0)^2}{4Dt} - [k - \overline{h}]t - \frac{\beta}{2}(x - x_0)t - \frac{\beta^2}{12}Dt^3. \tag{3.95}$$

We can now determine the wave speed c by imposing the condition $G(x(t),t) = 0$. This leads to a quadratic equation with positive solution

$$x(t) = x_0 + D\beta t^2 + 2Dt\sqrt{\frac{k-\overline{h}}{D} + \frac{\beta^2}{3}t^2}$$
$$= x_0 + \overline{c}t\sqrt{1 + \frac{4\beta^2 D^2 t^2}{3\overline{c}^2}} + D\beta t^2$$

with $\overline{c} = 2\sqrt{D(k-\overline{h})}$. Finally, differentiating both sides with respect to t yields

$$c \equiv \dot{x}(t) = \overline{c}\sqrt{1+\Gamma_0\beta^2 t^2} + \frac{\overline{c}\Gamma_0\beta^2 t^2}{\sqrt{1+\Gamma_0\beta^2 t^2}} + 2D\beta t, \tag{3.96}$$

where $\Gamma_0 = 4D^2/(3\overline{c}^2)$. For sufficiently small times such that $D\beta t \ll 1$, we have the approximation

$$c \approx \overline{c} + 2D\beta t + \frac{2(D\beta t)^2}{\overline{c}}. \tag{3.97}$$

Figure 3.13 shows example plots of the time-dependent wave speed for various choices of the activation rate k. It can be seen that there are significant changes in speed over a time course of 100 s, which is comparable to the time a wave would travel along a dendrite of a few hundred microns. In principle, it should be possible to test experimentally the predictions of the above analysis by initiating a translocation wave at different points along a dendrite and determining the corresponding wave speed.

3.3 Appendix: Pulled and Pushed Fronts

In this appendix, we review some of the basic properties of fronts propagating into unstable states. For a much more detailed account, see the review by van Saarloos [544] and Chap. 4 of [422]. For concreteness, we focus on a slight generalization of the Fisher–KPP equation

$$\frac{\partial u}{\partial t} = \frac{\partial^2 u}{\partial x^2} + f(u), \quad f \in C^1[0,1], \quad f(0) = f(1) = 0, \tag{3.98}$$

for which the homogeneous fixed point $u = 0$ is unstable ($f'(0) > 0$) and $u = 1$ is stable ($f'(1) < 0$). We also assume that $f(u) > 0$ for all $u \in (0,1)$. We are interested in determining the longtime asymptotics of a front propagating to the right into the unstable state $u = 0$, given initial conditions for which $u(x,0) = 0$ for sufficiently large x. It is not possible to carry out an asymptotic analysis by simply moving to a traveling coordinate frame, since there is a continuous family of front solutions. However, considerable insight into the evolution of a localized initial condition can be obtained by linearizing about the unstable state.

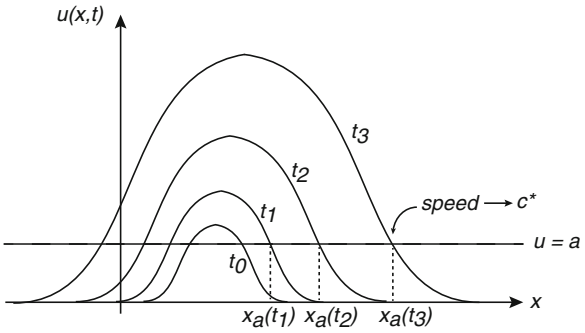

Fig. 3.14 Illustrative sketch of the growth and spreading of a solution $u(x,t)$ of the Fisher equation linearized about the unstable state $u = 0$, given a localized initial condition $u(x,t_0)$

3.3.1 The Linear Spreading Velocity

Linearizing (3.98) about $u = 0$,

$$\frac{\partial u}{\partial t} = \frac{\partial^2 u}{\partial x^2} + f'(0)u. \tag{3.99}$$

Substitution of the Fourier mode $e^{-i\omega t+ikx}$ gives the dispersion relation

$$\omega(k) = i(f'(0) - k^2). \tag{3.100}$$

The state $u = 0$ is then said to be linearly unstable if $\mathrm{Im}[\omega(k)] > 0$ for some range of k-values. In the case of the Fisher–KPP equation, after writing $k = k_r + ik_i$, this will occur when $f'(0) + k_i^2 > k_r^2$. Consider some generic initial condition $u(x,0)$ that is sufficiently localized in space (to be made precise later). Since there exists a range of unstable linear eigenmodes, we expect the localized initial condition to grow and spread out within the linear regime, as illustrated in Fig. 3.14. Tracking the evolution of a level curve $x_a(t)$ with $u(x_a(t),t) = a$, the *linear spreading velocity* c^* is defined to be the asymptotic speed of the point $x_a(t)$ in the rightward moving edge (assuming it exists):

$$c^* = \lim_{t\to\infty} \frac{dx_a(t)}{dt}. \tag{3.101}$$

The linearity of the underlying evolution equation (3.99) means that c^* is independent of the value a. (Note that for an isotropic medium, the leftward moving edge moves with the same asymptotic speed but in the opposite direction.) Suppose that c^* is finite. If we were to move in the traveling coordinate frame $\xi = x - c^*t$, then the leading rightward edge would neither grow nor decay exponentially. Imposing this condition on the Fourier expansion of the solution $u(x,t)$ then determines c^* in terms of the dispersion curve $\omega(k)$. More specifically, denoting the Fourier transform of the initial condition $u_0(x) = u(x,0)$ by $\tilde{u}_0(k)$, we have

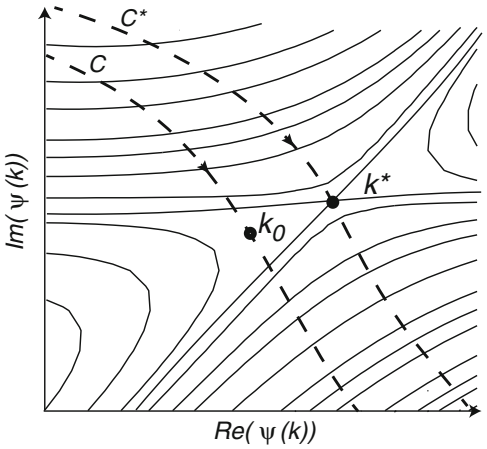

Fig. 3.15 Method of steepest descents. Sketch of $\mathrm{Re}(\psi)$ contours in the complex k-plane for an analytic function in the region of a saddle point at k^*. The integration contour C is deformed so that it passes through the saddle point

$$\begin{aligned} u(x,t) &= \int_{-\infty}^{\infty} \tilde{u}_0(k) \mathrm{e}^{i[kx-\omega(k)t])} \frac{dk}{2\pi} \\ &= \int_{-\infty}^{\infty} \tilde{u}_0(k) \mathrm{e}^{ik\xi} \mathrm{e}^{-i[\omega(k)-c^*k]t)} \frac{dk}{2\pi} \\ &= \int_{-\infty}^{\infty} \tilde{u}_0(k) \mathrm{e}^{ik\xi} \mathrm{e}^{\psi(k)t} \frac{dk}{2\pi}, \end{aligned} \tag{3.102}$$

where

$$\psi(k) = -i[\omega(k) - c^*k] = \omega_i(k) - c^*k_i - i[\omega_r(k) - c^*k_r] \tag{3.103}$$

In the limit $t \to \infty$ with ξ finite, we can approximate this integral using steepest descents. For the moment, we assume that $\tilde{u}(k)$ is an entire function (analytic in every finite region of the complex plane) so that we can deform the contour in the complex k-plane, that is, $(-\infty,\infty) \to C$, with C linking points at infinity in the complex plane where $\mathrm{Re}(\psi) < 0$.

Method of steepest descents. We briefly describe the method of steepest descents for a general analytic function $\psi(k)$; see also Fig. 3.15 and [275]. First, one would like to choose C so that the maximum of $\psi_r \equiv \mathrm{Re}(\psi)$ along the contour at k_0, say, is as large as possible, since this point will dominate the integral. Recall, however, that one of the Cauchy–Riemann conditions on an analytic function is that $\nabla^2(\mathrm{Re}(\psi)) = 0$, which means that $\mathrm{Re}(\psi)$ cannot have any maxima or minima (except at singularities or branch points where ψ would be nonanalytic). Therefore $\nabla(\mathrm{Re}(\psi)) = 0$ only at saddle points. Second, for a general integration contour, evaluating the integral in a neighborhood of the point k_0 will overestimate the value of the integral, since it does not take into account cancellations due to the rapidly oscillating function $\mathrm{e}^{i\mathrm{Im}(\psi(k))}$. The latter issue can be eliminated by choosing the contour that is the path of steepest ascent to a saddle point and the steepest descent away from the saddle. (If there exists more than one saddle, then one chooses the "highest" one). By construction, the path is parallel to $\mathrm{Re}(\psi)$. Hence, from the Cauchy–Riemann conditions, $\nabla(\mathrm{Im}(\psi)) = 0$

so that $\psi_i \equiv \mathrm{Im}(\psi)$ is constant along the contour. In other words, there are no fast oscillations along the path of steepest ascent and descent and one can obtain a good estimate of the integral by Taylor expanding about the saddle point. Thus, taking $\psi_i(k) = \psi_i(k^*)$ along C^*, we have

$$\begin{aligned} I &\equiv \int_{-\infty}^{\infty} \tilde{u}_0(k) \mathrm{e}^{ik\xi} \mathrm{e}^{\psi(k)t} \frac{dk}{2\pi} \\ &= \int_{C^*} \tilde{u}_0(k) \mathrm{e}^{ik\xi} \mathrm{e}^{\psi(k)t} \frac{dk}{2\pi} \\ &\approx \tilde{u}_0(k^*) \mathrm{e}^{i\psi_i(k^*)t} \int_{C^*} \mathrm{e}^{ik\xi} \mathrm{e}^{\psi_r(k)t} \frac{dk}{2\pi}. \end{aligned}$$

Finally, we Taylor expand $\psi_r(k)$ to second order in $\Delta k = k - k^*$, noting that $\psi'(k^*) = 0$ and $\psi_r''(k^*) < 0$ at the saddle,

$$\psi_r(k) = \psi_r(k^*) + \frac{(\Delta k)^2}{2} \psi_r''(k^*),$$

and approximate the remaining contour integral by a Gaussian. This then gives

$$I \approx \frac{1}{\sqrt{4\pi D t}} \tilde{u}_0(k^*) \mathrm{e}^{i[k^*\xi + \psi_i(k^*)t]} \mathrm{e}^{-\xi^2/4Dt} \mathrm{e}^{\psi_r(k^*)t}, \tag{3.104}$$

where $D = -\psi_r''(k^*)/2$.

Let us now apply steepest descent to the integral (3.102) for $\psi(k)$ given by (3.103) such that $\psi_r(k) = \omega_i(k) - c^* k_i$ and $\psi_i(k) = -[\omega_r(k) - c^* k_r]$. At the (unique) saddle point k^* at which $\psi'(k^*) = 0$, we have

$$c^* = \left. \frac{d\omega(k)}{dk} \right|_{k=k^*}. \tag{3.105}$$

Moreover, equation (3.104) becomes

$$I \approx \frac{1}{\sqrt{4\pi D t}} \tilde{u}_0(k^*) \mathrm{e}^{i[k^*\xi - [\omega_r(k^*) - c^* k_r^*]t]} \mathrm{e}^{-\xi^2/4Dt}, \tag{3.106}$$

where

$$D = -\frac{1}{2} \omega_i''(k^*). \tag{3.107}$$

Finally, we can determine the linear spreading velocity c^* by requiring that the asymptotic solution neither grows nor decays with time, $\psi_r(k^*) = 0$, which implies

$$c^* = \frac{\omega_i(k^*)}{k_i^*}. \tag{3.108}$$

Note that equating real and imaginary parts in (3.105) and combining with (3.108) means that we have three equations in the three unknowns c^*, k_r^*, k_i^*. In the particular case of the Fisher–KPP equation (3.98),

$$k_r^* = 0, \quad k_i^* = \sqrt{f'(0)}, \quad c^* = 2\sqrt{f'(0)}, \quad D = 1. \tag{3.109}$$

Since $k_r^* = 0$, we can combine (3.105) and (3.108) into the single condition $c^* = c(\lambda^*)$, $\lambda^* = k_i^*$, where

$$c(\lambda) = \frac{\omega_i(i\lambda)}{\lambda}, \quad \left.\frac{dc(\lambda)}{d\lambda}\right|_{\lambda=\lambda^*} = 0. \tag{3.110}$$

It can also be seen that the modulus of u falls off as

$$|u(x,t)| \sim \frac{1}{\sqrt{t}} \mathrm{e}^{-\lambda^* \xi} \mathrm{e}^{-\xi^2/4t}. \tag{3.111}$$

A more direct way to derive the function $c(\lambda)$ is to consider the linearized PDE in the moving frame $\xi = x - ct$,

$$-c\frac{dU}{d\xi} = \frac{d^2U}{d\xi^2} + f'(0)U,$$

and to assume the leading-edge solution $U(\xi) \sim \mathrm{e}^{-\lambda\xi}$.

In the above analysis, it was assumed that the Fourier transform of the initial condition $u_0(x)$ was an entire function. This would apply to cases for which $u_0(x)$ is a Dirac delta function, has compact support, or decays faster than any exponential for large enough x (e.g., a Gaussian). Now suppose that $u_0(x)$ falls off exponentially for large x, $u_0(x) \sim \mathrm{e}^{-\lambda x}$ for some λ. Then $\tilde{u}_0(k)$ has a pole in the upper-half complex plane at $k = k'$ with $\mathrm{Im}(k') = \lambda$. It follows that when deforming the contour C in the complex k-plane in order to perform steepest descents, we pick up a contribution from the pole. Taking this into account, it can be shown that, within the linear regime, initial conditions whose exponential decay rate $\lambda > \lambda^*$ lead to profiles that asymptotically spread with the linear spreading velocity v^*. On the other hand, if $\lambda < \lambda^*$ then the profile advances at a speed faster than c^* [544].

So far we have investigated the evolution of a localized initial condition in the linear regime. It still remains to determine whether or not there are classes of initial conditions under which the full nonlinear system converges to a unique asymptotic front solution and how the speed of the front c is related to the linear spreading velocity c^*. It turns out that for front propagation into a linearly unstable state, there are only two possibilities when starting from sufficiently steep initial conditions, that is, initial conditions that fall off faster than $\mathrm{e}^{-\lambda^* x}$ [544]:

Pulled front: $c = c^*$ so that the front dynamics is determined by the behavior in the leading edge of the front where $u(x,t) \approx 0$, that is, the front is pulled along by the linear spreading of small perturbations into the linearly unstable state.

Pushed front: $c > c^*$ so that nonlinearities play an important role in determining the velocity of the front, pushing it into the unstable state.

In the special case of initial conditions with compact support, it can be proven that the solution evolves into a front that propagates at the minimal possible wave speed $c_{\min}$, which is bounded above and below [15]:

$$c^* = 2\sqrt{f'(0)} \leq c_{\min} < 2\sqrt{\sup_u \left[\frac{f(u)}{u}\right]}. \tag{3.112}$$

For any concave function, $f(u) \leq uf'(0)$, the lower and upper bounds coincide and we have a pulled front; this applies to the standard Fisher–KPP equation where $f(u) = u(1-u)$. On the other, the upper and lower bounds do not coincide for concave $f(u)$. The minimal front velocity can then be larger than the linear velocity indicative of a pushed front. An example of the latter is the Ginzburg–Landau term $f(u) = u(1-u)(1+\alpha u)$ with $\alpha > 0$. One finds that for compact initial conditions, a pulled front is selected when $\alpha \leq 2$, whereas a pushed front is selected when $\alpha > 2$ [33].

3.3.2 Variational Method for Front Velocity Selection

Over recent years a number of methods have been developed to tackle the general problem of front velocity selection, that is, which of the infinity of possible wave speeds is selected by a given initial condition. One method analyzes the dynamics of the front position using Hamilton–Jacobi theory. Although it is only applicable to pulled fronts, it has the advantage of being able to tackle the effects of heterogeneities, as illustrated in Sect. 3.2.4 for CaMKII translocation waves. Here we briefly describe another method due to Benguria and Depassier [36], which is based on a variational principle. The latter can be applied to both pulled and pushed fronts, although in many cases it only provides lower and upper bounds for the front velocity. Consider a front solution of the reaction–diffusion Eq. (3.98) in traveling wave coordinates,

$$u_{\xi\xi} + cu_\xi + f(u) = 0, \tag{3.113}$$

with $\lim_{\xi\to-\infty} u(\xi) = 1$ and $\lim_{\xi\to\infty} u(\xi) = 0$, $\xi = x - ct$. Set $q(u) = -u_\xi > 0$ for $u \in (0,1)$, so that (3.113) becomes

$$q(u)\frac{dq}{du} - cq(u) + f(u) = 0, \quad q(0) = 0, \quad q(1) = 0. \tag{3.114}$$

Let $g \in C^1[0,1]$ be a positive, monotonically decreasing function with $\int_0^1 g(u)du < \infty$, and set $h = -g' > 0$. We denote the space of admissible functions g by the domain $\mathscr{D}$. Multiplying (3.114) by g/q and integrating with respect to u gives (after integration by parts)

$$\int_0^1 \left(h(u)q(u) + \frac{f(u)}{u}g(u)\right)du = c\int_0^1 g(u)du. \tag{3.115}$$

For fixed u, the functional

$$\Phi[q] = qh + \frac{f}{q}g$$

has a minimum at $q_0 = \sqrt{fg/h}$ with $\Phi[q_0] = 2\sqrt{fgh}$. It follows that

$$c\int_0^1 g(u)du = \int_0^1 \Phi[q(u)]du \geq 2\int_0^1 \sqrt{f(u)g(u)h(u)}du,$$

that is,

$$c \geq 2\frac{\int_0^1 \sqrt{f(u)g(u)h(u)}du}{\int_0^1 g(u)du} \equiv I[g]. \tag{3.116}$$

As we show below, there exists a function $\hat{g} \in \mathscr{D}$ that maximizes the lower bound for c in such a way that the equality holds. Hence, we have the variational principle

$$c = \max_{g\in\mathscr{D}} \left(2\frac{\int_0^1 \sqrt{f(u)g(u)h(u)}du}{\int_0^1 g(u)du} \right), \tag{3.117}$$

which can be used to estimate c using a parameterized set of trial functions. This result can also be used to derive the upper bound of (3.112) [36].

In order to establish the existence of the function $\hat{g}$, we first require $\Phi[q] = \Phi[q_0]$ for all u, that is, $hq = f\hat{g}/q$. Combined with (3.114) this gives

$$-\frac{\hat{g}'}{\hat{g}} = \frac{c}{q} - \frac{q'}{q},$$

which can be integrated to yield

$$\hat{g}(u) = q(u)\exp\left(\int_u^{u_0} \frac{c}{q(u')}du'\right) \tag{3.118}$$

for some u_0, $0 < u_0 < 1$. Since $\hat{g} > 0$ on $(0,1)$ and $h = \hat{g}f/q^2 > 0$ we deduce that $\hat{g} \in C^1[0,1]$ and is a positive, decreasing function. It remains to check that $\int_0^1 \hat{g}(u)du < \infty$, which requires determining the behavior near $u = 0$. Linearizing (3.113) around $u = 0$ shows that if $u \sim \mathrm{e}^{-\lambda\xi}$ for $\xi \to \infty$ with $\lambda = (c + \sqrt{c^2 - 4f'(0)})/2$, then $q \sim \lambda u$ for $u \sim 0$. The integral solution for $\hat{g}$ then implies that

$$\hat{g} \sim \lambda \frac{1}{u^{c/\lambda - 1}}, \quad u \sim 0.$$

Therefore, if $c < 2\lambda$, that is, $c > 2\sqrt{f'(0)}$, then $\int_0^1 \hat{g}(u)du < \infty$ and $\hat{g} \in \mathscr{D}$. Finally, in the special case $c = 2\sqrt{f'(0)}$, one can take the set of trial functions $g_\alpha(u) = \alpha u^{\alpha-1}$ with $g_\alpha \in \mathscr{D}$ for $0 < \alpha < 1$ and show that $I[g_\alpha] \to 2\sqrt{f'(0)}$ as $\alpha \to 0$. This means $c = 2\sqrt{f'(0)} \geq \max_g I[g] \geq 2\sqrt{f'(0)}$, that is, $c = \max_g I[g]$.